Smart Multifunctional Sutures for Advanced Healthcare

by

Tavia Walsh

B.A.Sc, University of British Columbia, 2018

A Thesis Submitted in Partial Fulfillment of the

Requirements for the Degree of

MASTER OF APPLIED SCIENCE

in the Department of Mechanical Engineering

© Tavia Walsh, 2020

University of Victoria

All rights reserved. This thesis may not be reproduced in whole or in part, by photocopying or other means, without the permission of the author.

Smart Multifunctional Sutures for Advanced Healthcare

by

Tavia Walsh

B.A.Sc, University of British Columbia, 2018

Supervisory Committee

Dr. Mohsen Akbari, Supervisor,

(Department of Mechanical Engineering)

Dr. Keivan Ahmadi, Departmental Member,

(Department of Mechanical Engineering)

Supervisory Committee

Dr. Mohsen Akbari, Supervisor,

(Department of Mechanical Engineering)

Dr. Keivan Ahmadi, Departmental Member,

(Department of Mechanical Engineering)

ABSTRACT

Recent advances in the miniaturization of biosensors and drug delivery systems have allowed for the continuous and non-invasive monitoring of patient health. While sutures are mainly used for approximating tissues in clinical practice, there has been emerging development of new suture materials for improving wound healing outcomes. We report a novel method of continuous and high-throughput fabrication of multifunctional sutures and threads which allows for control over a wide range of important microstructural and physical properties. In the proposed fabrication method, a thread or suture is spooled across a base collecting plate. The fabrication method involves direct electrospinning (ES) onto the surface of threads and sutures. ES has also been widely used within the area of biomedical and tissue engineering, given its compatibility with a range of synthetic and natural biocompatible polymers. As the thread moves beneath a syringe pump and a spinerette needle that is positively charged, electrospun nanofibers collect on the surface of the thread. The coating layer thickness and the alignment of the nanofibers with the direction of the thread is tuned

by varying the spooling speed and the distance between the spinerette needle and the thread. The resulting smart sutures have applications in both passive and on-demand drug release, durable wound biosensing, and improved cell viability and attachment. These structures may be manipulated in different materials (i.e. skin, fabrics, wound dressings) and be combined using textile methods (e.g. braiding, weaving, knitting) to form three dimensional (3D) constructs.

Contents

List of Tables

List of Figures

ACKNOWLEDGEMENTS

I would like to sincerely thank my supervisor, Dr. Mohsen Akbari, for his guidance during my work at the Laboratory for Innovations in Microengineering and for demonstrating confidence and encouragement for his students professional and academic success. I am incredibly grateful for all the opportunities that I have received at LiME lab and at the University of Victoria. I would also like to acknowledge my fellow lab mates at the Laboratory for Innovations in Microengineering. Thank you all for being so generous with your time and knowledge. Finding a better group of colleagues would be impossible.

DEDICATION

This thesis is dedicated to my family, Catherine, Bruce, and Rowan, and sisters-in-arms, Annie, Lauren, and Tania. Your support means the world.

Chapter 1

Introduction

This chapter provides a background into the existing literature on the topics of medical sutures used for wound closure and implementation of ES technology in biomedical applications, including a review on the current work in thread-based biosensing, drug release, and tissue engineering. The components of this thesis are introduced by an overview of the document itself.

1.1 Commercial suture technologies

Surgical sutures facilitate the closure of wounds induced by trauma or surgery by holding the wound edges together. Sutures are also used as fixation methods to anchor devices and implants in place within the body [1]. Important surgical suture characteristics include secure knotting ability, minimal trauma resulting from insertion, suture strength, risk of infection, biocompatibility, biotoxicity after biodegradation, and the healing properties of the sutured tissues, all of which must be considered when determining the optimal type of suture for wound closure or device fixation [6]. Medical sutures (shown in Figure 1.1) are broadly classified into either absorbable or permanent, synthetic or naturally-derived material, and via the physical configuration

of the strands (monofilament, multifilament, twisted, and braided) [1, 7].

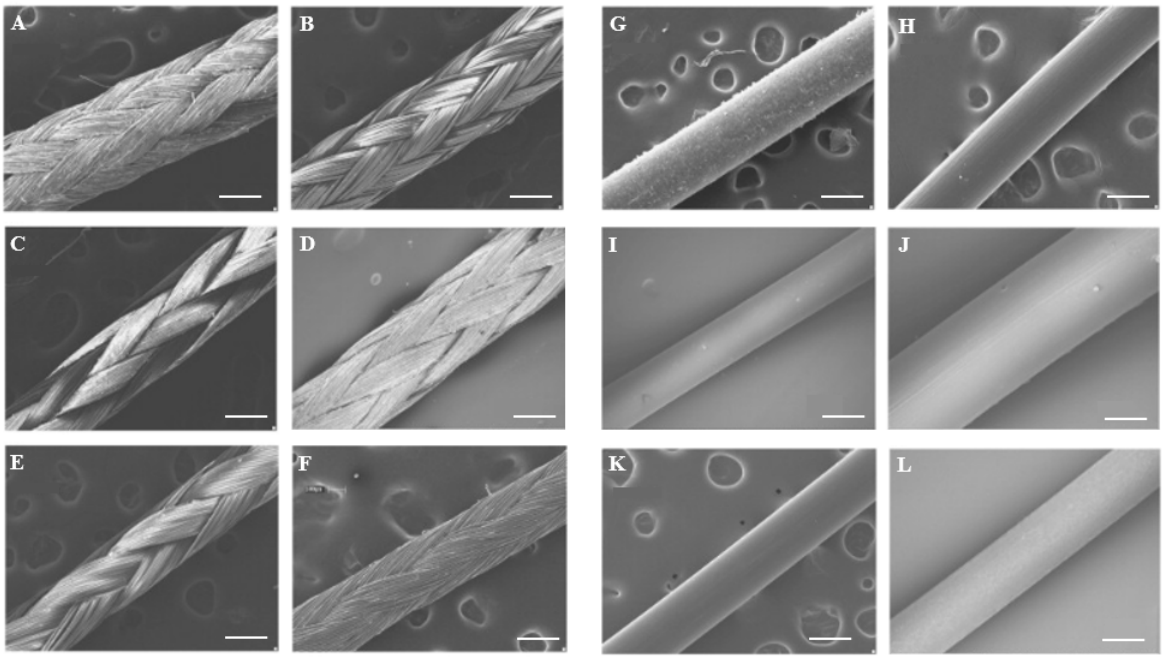

Figure 1.1: SEM (scanning electron microscope) images of common commercial suture surface topography. Multifilament (A) silk (natural fibers), (B) poly(glycolide/L-lactide) copolymer, (C) polyglycolide, (D) antimicrobial-coated polyglycolide, (E) poly (ethylene terephthalate), (F) nylon, and monofilament (G) chromic catgut (collagen derived from sheep intestinal submucosa), (H) polyester, (I) polybutester, (J) poly(glycolide/trimethylene carbonate) copolymer, (K,L) nylon (scale bars = 100μm) [1].

The physical configuration of sutures depends on the material type: nylon, polyester, and stainless steel sutures are readily available in multi- and monofilament forms, while natural origin catgut, collagen, and cotton sutures are generally only fabricated in multifilament form [1]. Braided multifilament configurations are additionally common for silk, polyester, and polyamide-based suture types [1]. When compared to monofilament versions, multifilament suture materials generally display greater tensile strength, pliability, and flexibility during handling and knot-tying [1]. The physical configuration of sutures also has a close relationship with many important biological effects. For example, multifilament suture configurations have been shown

to introduce wound infections, granulomas, and sinuses, when compared to monofilament versions of the same material, as their microfluidic capillary capacity may cause increased bacterial transport [6, 8].

Absorbable suture materials are defined as materials that retain their tensile strength for the required period of healing but lose the majority of the tensile strength within 2-3 months [1, 9]. With these closure devices, dissolving rates are paralleled with increasing tissue strength, and degradation occurs by proteolytic enzymatic degradation [9]. The recent development of new synthetic and longer-lasting absorbable sutures has pushed the tensile strength retention period beyond 2–3 months [1]. In contrast, nonabsorbable sutures will retain the majority of the initial tensile strength for a period longer than 3 months, and will remain in the tissues until removed by a healthcare practitioner [1, 9]. Nonabsorbable sutures are generally used for skin closure and visceral surgeries, as the cosmetic result is superior due to a reduced negative immune response [9].

While both synthetic and natural polymers have been used to fabricate suture threads, the advantages of consistency within the raw material source and reproducible manufacturing of synthetic polymers has driven the commercial demand towards these materials [1]. Further, the majority of research and development efforts in the area of sutures is directed towards absorbable synthetic materials, as well as sutures with multifunctional capabilities (e.g. antimicrobial coatings) to reduce the chance of infection [1]. Other suture properties that relate to the morphology of the suture surface are being developed; for example, barbed sutures and flat "ribbon-like" sutures are newly approved for commercial use, and eliminate the need for knot typing in deep surgical regions while also reducing the risk of tissue strangulation [10]. While sutures in clinical use are mainly simple physical entities used for fixture and approximating tissues, the recent growth in the development of different classes of

suture materials for improved healing outcomes via (chemical and physical) surface modification methods plays upon the inherent versatility of the technology.

1.1.1 Wound healing & sutures

Wounds are characterized by superficial lacerations or penetration to underlying tissues, arising from physical injuries, diseases, or surgical interventions [11]. For most injuries, the bodily healing response occurs in four highly programmed and controlled stages, namely hemostasis, inflammation, new tissue formation through proliferation, and remodelling [11]. These consecutive stages are orchestrated by different cell populations such as neutrophils, macrophages, and fibroblasts, and molecular mechanisms of wound repair such as extracellular matrix (ECM) proteins, peptide growth factors, and hormones [11, 12]. The four phases must occur in the proper sequence and time frame for successful wound healing. If the wound healing response is impaired, a wound can become chronic with excessive levels of proinflammatory cytokines, a deficiency of stem cells, and the potential existence of persistent infection and drug-resistant microbial biofilms [13]. Other complexities of wound healing include the various levels of wound strength during the process of healing, the presence of biomaterials and foreign bodies, and the type of surgical incision (which have differing healing issues) within a surgical context [1].

When a foreign object such as a suture material is introduced to a wound for the purposes of wound closure, the body's inflammatory reaction (i.e. foreign body reaction) is initiated. The body initiates a chain of inflammation, where the two main macrophage sub-types (M1 and M2) play a central and critical role in wound healing at the site of the foreign body [14]. However, when prolonged wound inflammation shows no subsequent anti-inflammatory peak, it results in a delayed wound healing response [15]. This early imbalance of immune reactions can jeopardise wound healing

success, therefore persistent pro-inflammation is expected to impair wound healing at the site of the surgical suture implantation. Uff et al. demonstrated that sutures release immunotoxic factors which considerably influence macrophage behaviour *in vitro* [16]. As macrophages are central to the inflammatory response and act to coordinate wound healing, this interaction with immune competent cells affects localized immunity. In an *in vitro* study with human monocyte/macrophage THP-1 cells of the relative gene expression of four inflammatory cytokines (IL-1β, IL-1α, TNFα, IL-8) and one cell surface marker (CCR7), a variety of absorbable and non-absorbable sutures either caused an upregulation of pro-inflammatory marker genes or remained reasonably inert [14]. Further, in a study by Andrade et al., different suture materials were observed to induce both differentiated tissue reactions and morphological surface changes [17]. Researchers observed that the induced differentiated tissue reactions of the suture materials were dependant on the chemical properties of suture material, which suggests the need for individualized indications for each suture material.

The use of sutures as implanted wound closure devices is appropriate if the depth of injury is presumed to lead to excess scarring, which occurs when the wound edges are not properly opposed (typical to lacerations extending through the dermis layer) [18]. Wound healing with closure is categorized into three clinical methods: primary, secondary, and tertiary intention closure (Figure 1.2) [18]. Immediate postoperative closure of wounds (primary wound closure) is the closure of a clean and uncontaminated laceration wound via suturing. This operative closure creates a functional scar with complete healing, however is limited to only a small window of opportunity for closure (4-8 hr) [18]. These types of small and clean wounds are usually associated with a short hemostatic and inflammatory phase duration as blood clot formation is limited to wound sealing and minor cell debris clearing [12]. Some higher injury wounds must be deliberately left open to allow for the wound margins to increase

on high-tension areas (i.e. over joints or areas with a thick dermis, such as on the back) of the body. Typically, these wounds will heal slowly by secondary intention, without surgical closure [18]. Tertiary intention (or delayed primary intention) wound closure via suturing is utilized for wounds that are irregular, contaminated, and/or infected [12]. Large, contaminated, and infected wounds require more time to heal as the initial phases of wound healing include periods of hemostasis and removal of cell debris and necrotic tissue before granulation tissue formation begins [12], so a delayed period before closure is required. In such cases, sutures with localized antibiotic and/or growth factor drug delivery may help to improve healing outcomes by reducing the bacterial load in deep regions of the wound and facilitate faster healing outcomes [19].

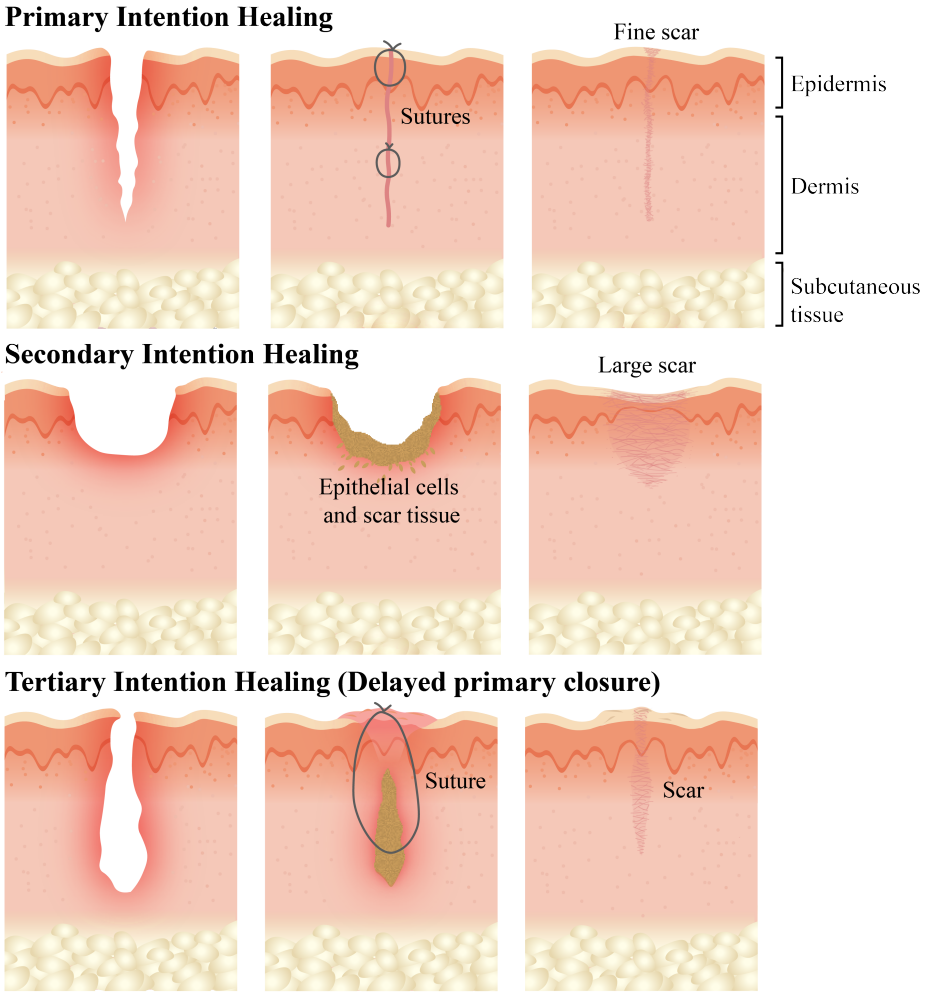

Figure 1.2: Wound healing by primary, secondary, and third intention and the suture placement for facilitating wound closure.

1.2 Suture applications in biomedical engineering

While sutures are among the most widely used devices in clinical medicine, most existing commercial varieties use the thread-like geometries for purely mechanical structures that are stress resistant and flexible. However, these current technologies lack the ability for programmable actuation or sensory feedback control. Sutures with embedded flexible sensors and the associated electronic circuits may be able to perform these functions in addition to their required mechanical functions [20]. Recent

technological advances in the miniaturization of sensors and drug releasing components have progressively altered the health care system by allowing for the continuous monitoring and treatment of patients' health status. Fabrication methods such as photolithography, screen-printing, and stamping are common approaches for the implementation of electrodes onto planar surfaces [21]. Specialized and localized drug dosing requirements have driven micro- and nano-fabricated implantable drug delivery systems, such as microfluidics, microneedles, and micropumps, fabricated using traditional lithography processes. However, these microfabrication processes can often be costly and time consuming [21]. Therefore, sensor and drug releasing fabrication methods involving economical and highly scalable thread and suture materials present an area of great research interest [22]. Functionalized thread and suture-based biotechnologies have also recently emerged as methods for tissue constructs and biomedical implants [23, 24]. As threads are naturally thin and flexible, they can be easily manipulated into complex 1D (one dimensional) to 3D shapes using traditional textile processing methods [25, 26].

1.2.1 Sutures for drug delivery

Significant progress has been made in the identification of signaling molecules and their mechanisms of action in healthy and infected/non-healing wounds [27, 28]. There has been parallel interest in using these signals therapeutically to accelerate healing rates or enable improved healing that would not occur naturally in chronic wounds. Delivery systems for proteins, genes, small, and large molecule drugs in the context of localized wound healing have several requirements. First, these delivery systems must maintain the bio-availability of the therapeutic and protect against protein breakdown at the site of the wound [29]. The prevention of rapid release into wound exudates, protecting the bioactivity of the therapeutic, is also of importance

[29]. The cumulative release and duration of release within the wound must occur at a physiologically and clinically relevant rate. Successful localized drug delivery systems would minimize the required dosage and frequency of application required for effective wound healing [29]. Controlled drug delivery has further advantages over normal dosages, included a reduction in dosage frequency, localized therapeutic effect, and enhanced patient compliance [30].

Interestingly, a literature review of thread and fiber-based drug delivery showed that research has been primarily focused on drug release from (1) electrospun fibers [31, 32] or (2) suture-like constructs [33, 30]. Electrospun drug-loaded materials have been widely researched for applications such as pain relief [34], cell death-inducement [35], and water-soluble oromucosal delivery [36]. He et al. used aligned electrospun PLLA (poly-L-lactic acid) fiber collection to create twisted threads loaded with model drug tetracycline hydrochloride. The researchers showed a large initial burst release from their fibers, suggested to have applications for bacterial wound infections [31]. An investigation on a drug-loaded surgical thread with area-specific anesthesia delivery was performed by Hakim et al. [30]. The drug-loading and selective drug delivery was achieved by first coating threads in poly-dopamine, followed by adhesive functionalization of the suture surface with lidocaine. Results showed that with surface functionalization, the suture retained adequate mechanical properties and performance. The passive *in vitro* drug release and *in vivo* local analgesia was achieved one day after surgery and persisted for approximately one week in 80% of treated rats [30]. Da Silva et al. utilized chitosan yarns, a non-commercial suture material but with potential future use as biodegradable surgical sutures, to potentiate the wound healing process through the release of N-acetyl-D-glucosamine. These drug-loaded yarns were formed via a wet-spinning process (extrusion of solution into a coagulating bath) and demonstrated gradual release over a 49-day period [33].

Electrospun polymeric nanofibers are a proven strategy for drug delivery system applications, as the high surface-to-volume ratio of the fibers improve processes such as drug loading and mass transfer [32]. The results of thread-based drug-release studies show passive release of antibiotics, analgesics, and other bioactive chemicals. Alternatively, if the amount of suture-released drug could be reduced through the use of targeted and on-demand drug release thread-based systems, this would potentially benefit wound healing outcomes by limiting the antibiotic resistance of bacteria in the wound, provide bioactive and growth factors at the correct stage of wound healing, and provide pain relief only when required by the user [30]. Therefore, drug-encapsulating materials and drug-releasing systems should be adapted to meet patient- and wound-specific drug release needs.

1.2.2 Sutures for biosensing

The biosensor miniaturization trend is being driven by increased portable device development in regards to the reduction or elimination of reagents, assay time, and energy consumption, and improvements in analysis efficiency and simplified operations [37]. Flexible bioelectronics and biosensors also enable a large variety of biomedical applications that would be otherwise unachievable with the use of conventional rigid electronics, as the high conformity of these devices to the effected area of the human body (e.g. wound beds) may yield better quality recordings of physiological events [38]. Mostafalu et al. report on a thread-based microfluidic network that can be interfaced with tissues in three dimensions. Physical and chemical sensors were integrated into the microfluidic network to monitor physiochemical tissue properties with direct integration with tissues. Functional threads are used as the building blocks of a thread-based diagnostic device, capable of measuring strain, pH, and glucose, and were fabricated via dip coating processes with various conductive and functionalized

inks [22]. Additionally, Sekar et al. recently developed a functionalized conductive carbon yarn for monitoring biomarkers in sweat [39]. The conductive yarn working electrode was fabricated using a similar dip coating and drying procedure, followed by the immobilization of specific antibodies to MNPs (magnetic nanoparticles) in the coating ink. Within the area of sutures, Kim et al. developed thin and flexible sensors and microheaters that could potentially act as surgical sutures for targeted wound monitoring [20]. The ribbon-like constructs were fabricated using conventional (photolithography, reactive ion etching) and unconventional (transfer printing, sacrificial release) fabrication methods. However, as demonstrated by the researchers, the knotting strength and knot holding abilities of these sutures were limited. Additionally, the traditional manufacturing processes required for these sensors and actuators can be expensive and time consuming. Conversely, Banerjee et al. detected blood plasma glucose and bovine serum albumin in an experimental setup in which commercial threads were used as both the fluid-transporting channels and colorimetric chemical reactors [40]. The researchers determined that the functionalized cotton and silk threads were suitable for incorporation into thread-based field-deployable disposable chemical reaction and sensing systems [40].

1.2.3 Sutures for tissue engineering

Tissue engineering is a multidisciplinary field in which researchers utilize various tools to fabricate tissue-like biological constructs; in addition to the goal of replacing diseased and/or damaged organs and tissues within the human body, engineered tissues may be used for diagnostic and therapeutic research purposes [41]. Threads, traditionally used in textile and apparel industries, have recently emerged as promising scaffolding materials for the fabrication of tissue constructs and biomedical implants for organ replacement and repair. Thread-based morphophysiological tissue

constructs have been widely studied and can be manipulated to model physiological tissues using various traditional fiber manufacturing and assembly methods. These fiber-based systems have been shown to demonstrate biomimicry of epithelial [42], skin [24], connective [43, 44, 45, 46], skeletal muscle [25, 47], smooth muscle [48], and nervous tissues [49], and offer flexibility in the areas of fiber size and length, fiber assembly, pore size, and multi-material composition. Notably, Fang et al. developed a braided silk fibroin scaffold for use in surgical tendon repair [50]. The braided scaffolds were seeded with primary tenocytes and implanted in a rabbit animal model, where they showed enhanced cell adhesion and propagation, with *in vivo* data confirming efficient neo-tendon formation with uniform and oriented bundles of collagen. In a study by Chen et al., the incorporation of hESC-MSCs (human embryonic stem cells) in a knitted silk-collagen scaffold, followed by *in vitro* mechanical stimulation, was shown to result in a highly efficient tissue-engineered tendon construct [45]. In this study, the cells displayed a pronounced spindle-shaped morphology when seeded on the knit scaffold and were appropriately elongated and aligned along the direction of mechanical stress. Recently, Li et al. fabricated an over-twisted helical yarn from electrospun fibers which simulated native mechanical complexities, onto which MSCs (mesenchymal stem cells) were seeded. Researchers proved that this yarn-based tissue construct meet requirements for the regeneration of tough tissues such as muscle, bone, and tendon [46].

1.3 Electrospinning technology

ES is a voltage-driven process for creating polymer fibers. The basic ES setup consists of a capillary through which a liquid polymer is forced via a syringe pump, gravitational forces, or pressurized gas, as well as a voltage source (positive or negative

polarity) that charges the liquid and a grounded collector [51]. ES is related to the process of electrospraying, but a number of processing parameters are optimized in order to generate solid fibers as opposed to solid polymer droplets [51]. ES enables the high-efficiency fabrication of ultra-thin fibers with a range of nano- and micro-diameter fibers possible. A broad range of materials can be processed by ES, with effective control over the resulting construct's morphology and structure (diameter, surface morphology, interior structure, etc.) [52], making ES a promising technology for a variety of applications.

Electrospun fiber formation is dominantly a self-assembling process; all features of the nanofiber are determined by this process and induced by electrostatic interactions [53]. The development of ES methods and materials has been characterised over a wide span of research; the electrohydrodynamic phenomena of ES and the initial fabrication method was patented in 1902 by Cooley and Morton, followed by additional patents by Formhals, which moved the ES technology in the direction of commercialization for the fabrication of fully-electrospun textile yarns [54]. As such, ES rapidly changed fiber-making into an economical method that could be done at a laboratory bench, with broad applicability in the areas of materials science, life sciences, and clinical medicine [2]. Following these development, wider ranges of organic polymers that could be electrospun into fibers were studied and developed by Reneker and Rutledge [55].

The conventional ES setup is configured with a stationary base collector, as shown in Figure 1.3A. In this system, a syringe pump is held at a set distance from an electrically grounded conductive base collector plate. A solvent, often organic, is used to dissolve the given polymers and/or a combination of polymers and additives into a liquid ES solution [56], which is loaded into the syringe. A positive voltage (5-35kV) is applied between a metallic needle attached to a syringe, through which liquid

polymer solution flows, and the base collector plate [2]. The electric field between the two charged surfaces causes the liquid polymer to form a solid and continuous fiber midair, which is then deposited onto the base collector plate. As the polymer exits the needle and the polymer solution is electrified under applied voltage, a tapering 'Taylor cone' is formed, shown in Figure 1.3B [2]. The polymer nanofibers then begin to form as they elongate into an electrified fluid jet. At the end of the straight jet segment, the jet goes through a series of successively smaller electrically driven coiling structures, including three stages of bending instabilities. The radius of each bending coil increases in diameter and follows a conical shaped trajectory, while the diameter of the fiber becomes thinner as the loop diameter increases. The fiber solidifies as the solvent component evaporates forming a continuous thin fiber midair, which is then deposited onto the conductive base collector [2]. Issues arise when the straight jet begins to become asymmetrical, as irregularities tend to grow further along the jet into larger bead-like structures, propagating along the fiber to become fiber deformations [53]. Branching instabilities that occur along the path of the jet are also observable and depend on the chosen ES parameters, which must be optimized for each unique ES setup and polymer [53].

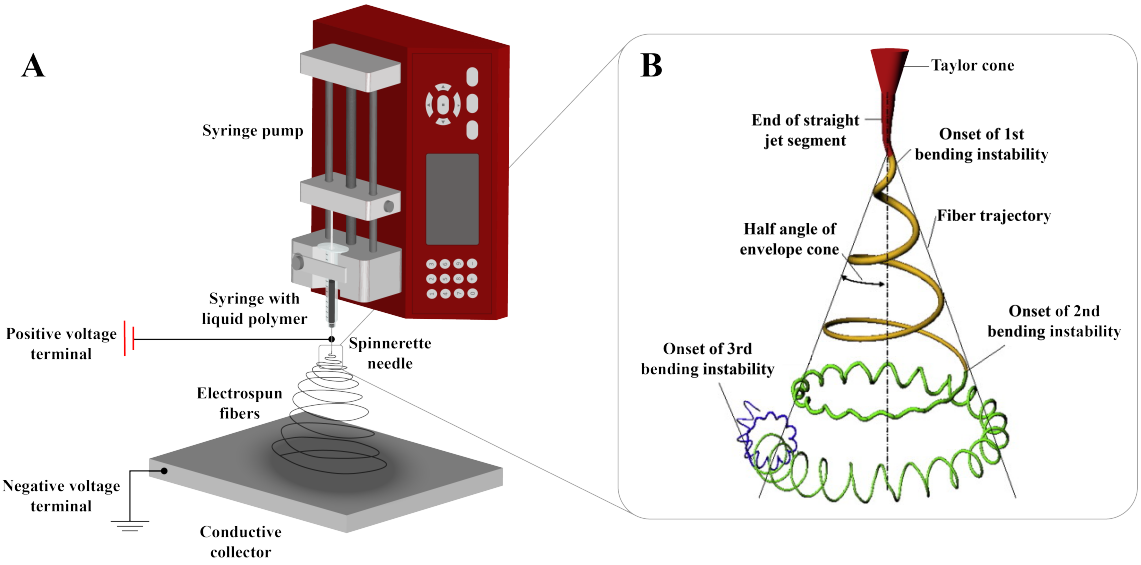

Figure 1.3: (A) Traditional ES setup. (B) Sequence of electrospun fiber formation [2].

The nanofibrous mats fabricated using a common ES setup (Figure 1.3A) will consist of randomly oriented and densely packed fibers. The shape, height, and alignment of the resulting scaffold, formed from layers of subsequently deposited electrospun fibers, depends on the direction of the electric field, which may be manipulated in different ways. For example, several modifications of the ES technology have been developed for enabling alignment of nanofibers, including the rotating drum [57], electrospun fiber pulling [58], and conductive patterned collectors [54, 59]. The ES process can be controlled to produce fibers with nanoscale diameters, various cross-sectional shapes, beading along the fiber length, branching, and zigzag formations [2]. Additions to the fluid ES polymer result in the chemical reagent, secondary polymer, dispersed nanoparticles, proteins and growth factors, and/or live cells, incorporation into the subsequent nanofiber [55]. Post-ES treatment further broadens the uses of the of the fibrous construct; these methods include chemical crosslinking, vapour coating, chemical treatment, and thermal processing [60].

The alignment of nanofibers has been proven to encourage ordered cell growth

along the matrix, generating patterns essential for their tissue and organ function [61]. The vast amount of research interest in ES has allowed for the combination of different properties such as fiber size, structure, morphology, alignment, porosity, core-sheath fibers, and triaxial fibers. This ability to tune the resulting electrospun structure has benefits for the recapitulation of molecular and structural properties of native ECM [61]. In addition, drug and other bioactive releasing electrospun fibers have been extensively researched, with the use of materials such as PNIPAm (Poly(N-isopropylacrylamide) [62], silk fibroin [63], gelatin [64], and their composites. The versatility of ES allows for biomedical devices to be coated with nanofibrous materials for applications in medical implants [65], micropatterned electrodes [66], and textile substrates [67]. The high adaptability of the ES technology and the commercial economics of thread-based biotechnologies make their combination of significant research interest. Additionally, the ability to fabricate nano-scale structures from raw materials, natural and synthetic polymers, and composites (consisting of organic and inorganic components) using ES demonstrates the efficacy of this technique for the preparation of various nanostructures for biomedical applications [55].

Constructs with rope-like geometries comprised fully of electrospun fibers have been developed by various groups. Researchers Theron, Zussman, et al. examined an electrostatic field-assisted assembly technique in combination with ES to position and align polymer-based electrospun fibers on a grounded wheel-like bobbin collector [3, 68]. This device wound a continuous fiber which collected at the rotating blade-like edge, resulting in compounded parallel arrays of nanofibers with a diameter range of 0.1-100μm (Figure 1.4A). Similarly, two metal blades were used to concentrate the deposition of aligned nanofibers by Teo et al., creating a bundle of highly aligned PCL (polycaprolactone) fibers, enabling the production of braided structures and twisted electrospun fiber ropes (Figure 1.4B) [4]. Zheng et al. report a novel method for fabri-

cating twisted electrospun yarns; directed by electrostatic interaction, the electrospun fibers were manipulated by a frame base collector separated by an insulating gap of variable width, then twisted together by manual rotation [69]. In another study, a continuous micron-scale fully electrospun rope comprised of two intercalated fibers was fabricated via a modified multi-nozzle rotating ES spinneret (Figure 1.4C) [5].

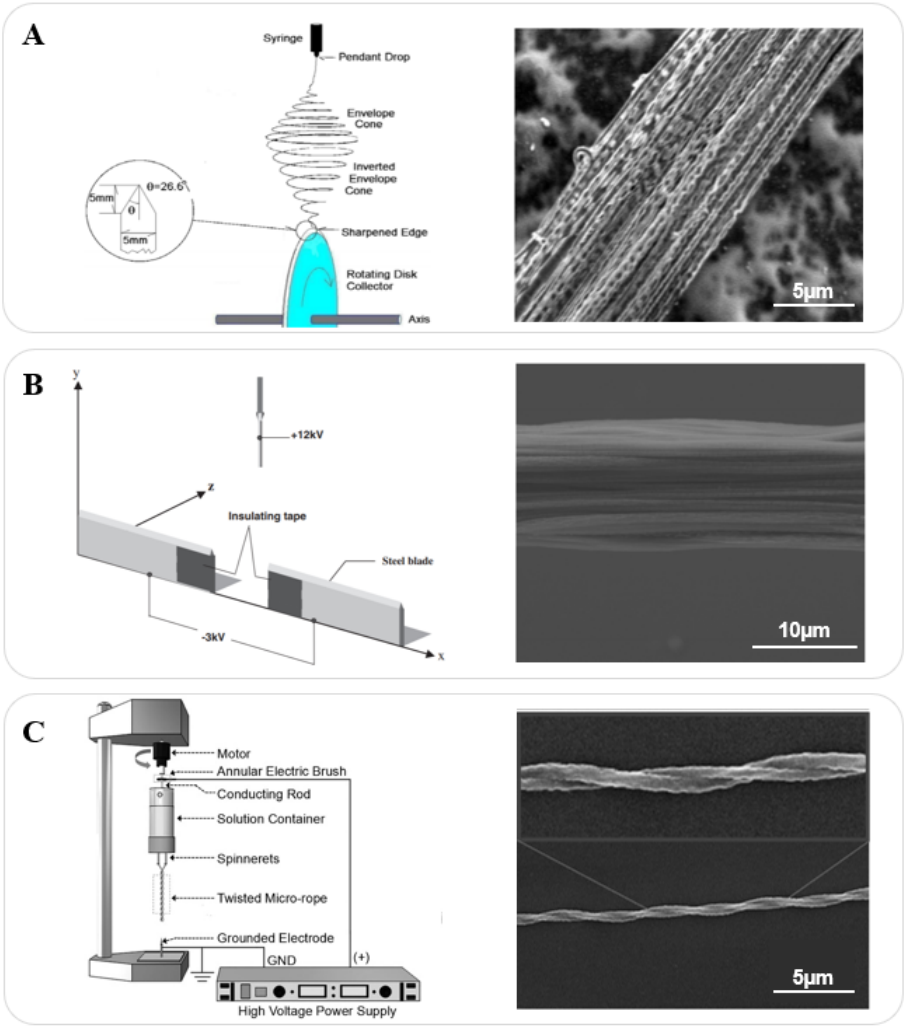

Figure 1.4: (A) ES setup and jet path with fiber deposition onto rotating disc edge and the resulting aligned NF yarn [3]. (B) Experimental setup for precise deposition of electrospun fibre on two blade edges and the resulting highly-aligned fiber bundle [4]. (C) Schematic of a rotating multi-nozzle ES emitter and the resulting two-fiber micron-scaled ropes [5].

These purely-electrospun thread fabrication methods have highly interesting applications in biomedical engineering; however, a method of using ES as a coating method hosts the following benefits. With the proposed method, one can create coated threads with multiple layers of different polymers with distinct physical and chemical properties. This method also allows for longer lengths of coated threads to be fabricated, as the purely-electrospun threads fabricated using the previously mentioned methods are constrained in length due to the size and design of the conductive collecting device. Additionally, the proposed method can employ commercial suture materials as the core thread, keeping the tensile strength, knotting strength, knotting flexibility, and regulatory approval required for wound closure applications. These benefits support the research and development of ES technologies for thread/suture coatings as an alternative to purely-ES thread fabrication methods.

1.4 Agenda

Chapter 1 provides a background on the topics of wound healing, commercial sutures used for wound closure, and implementation of ES technology in biomedical applications, including a review on the current work in thread-based biosensing, drug release, and tissue engineering. This section also contains an introduction into the components of this thesis by an overview of the document itself.

Chapter 2 describes the novel experimental ES setup used to fabricate the nanofibrous coated threads and sutures and defines the materials and methods used for the fabrication of the thread types. A feasibility study of the electrospun nanofibers, coating thickness, alignment, and tensile properties of PCL electrospun coatings is discussed.

Chapter 3 demonstrates the 1D-3D textile methods with which the nanofibrous

coated threads can be manipulated.

Chapter 4 characterizes stimuli-responsive electrically conductive and magnetic coatings.

Chapter 5 characterizes the results of two types of drug-releasing electrospun coated threads, and the experimental results of antibiotic-loaded thread coatings on cultured bacteria.

Chapter 6 describes the cell culture and experimental methodology for *in vitro* biocompatibility, cell attachment, and proliferation on three types of electrospun coated threads. Cell biocompatibility, attachment, and proliferation are evaluated.

Chapter 7 contains a restatement of the proposed fabrication method, claims, and results of the thesis. This section also enumerates avenues of future work for further development of the method and its future applications.

Chapter 2

Electrospinning setup & optimization

In this work, we present a novel approach for creating smart sutures by coating the surface of medical sutures with nanofibrous materials. The coating was achieved by continuous deposition of nanofibers using a modified ES device. With this method, the nanofibrous thread coating thickness and resulting electrospun fiber orientation is controlled by system parameters (spooling velocity, duration of ES, and thread-needle displacement) determined by the user, while the electrospun fiber diameter is dependant on polymer concentration and molecular weight which effect the ES polymer solution viscosity and electro-spinnability.

2.1 Proposed technology

The nanofibrous coated threads were prepared using a customized ES system. In this system, a programmable syringe pump (New Era Pump Systems, USA) was positioned above the base collector on a platform. ES solutions were loaded into syringes with blunted 18-gauge needles attached. The needle and base collector were attached

to the positive and negative terminals of a high voltage power supply (Gamma High Voltage Research, USA), respectively. A custom spooling system moved the thread horizontally beneath the syringe, above the collector plate at a set velocity. The syringe was held at a constant distance from the base collecting plate while the stationary thread is moved horizontally, within a movable range of 1-8cm (thread displacement) relative to the spinerette needle. The spooling setup consisted of a stepper motor (SparkFun Electronics, USA) controlled by an Arduino Uno (Arduino, USA) and Arduino Motor Shield Rev3 (Arduino, USA). An LCD (liquid crystal display) screen (HD44780, Adafruit, USA) and physical push-buttons make up the user interface, which allows for the spooling velocity and total run duration to be set by the user. All ES experiments were performed at room temperature (21°C) and relative environmental humidity.

The proposed fabrication method is shown in Figure 2.1A, where a thread or suture is spooled across a base collecting plate. As the thread moves beneath the charged spinerette needle, electrospun nanofibers collect onto the surface of the thread. The coating layer thickness and the alignment of the nanofibers with the direction of the thread can be tuned by varying the spooling speed and the distance between the spinerette needle and the thread. As shown in SEM cross-sectional images of coated threads, the threads may be coated with single (Figure 2.1B) or multiple layers (Figure 2.1C) with multiple spooling passes beneath the ES spinerette. While previous studies regarding electrospun scaffolds and yarns have mainly focused on purely-electrospun threads, we aim to demonstrate an expanded proof of concept for electrospun coated threads and sutures with a diverse range of applications. The resulting smart sutures can be applied to passive drug release, temperature responsive drug release, durable glucose and pH biosensing, cell viability and attachment, and be manipulated in different materials (e.g. skin, textile-based wound dressings, and

fabrics) and be combined together into 1D-3D constructs (Figure 2.1D).

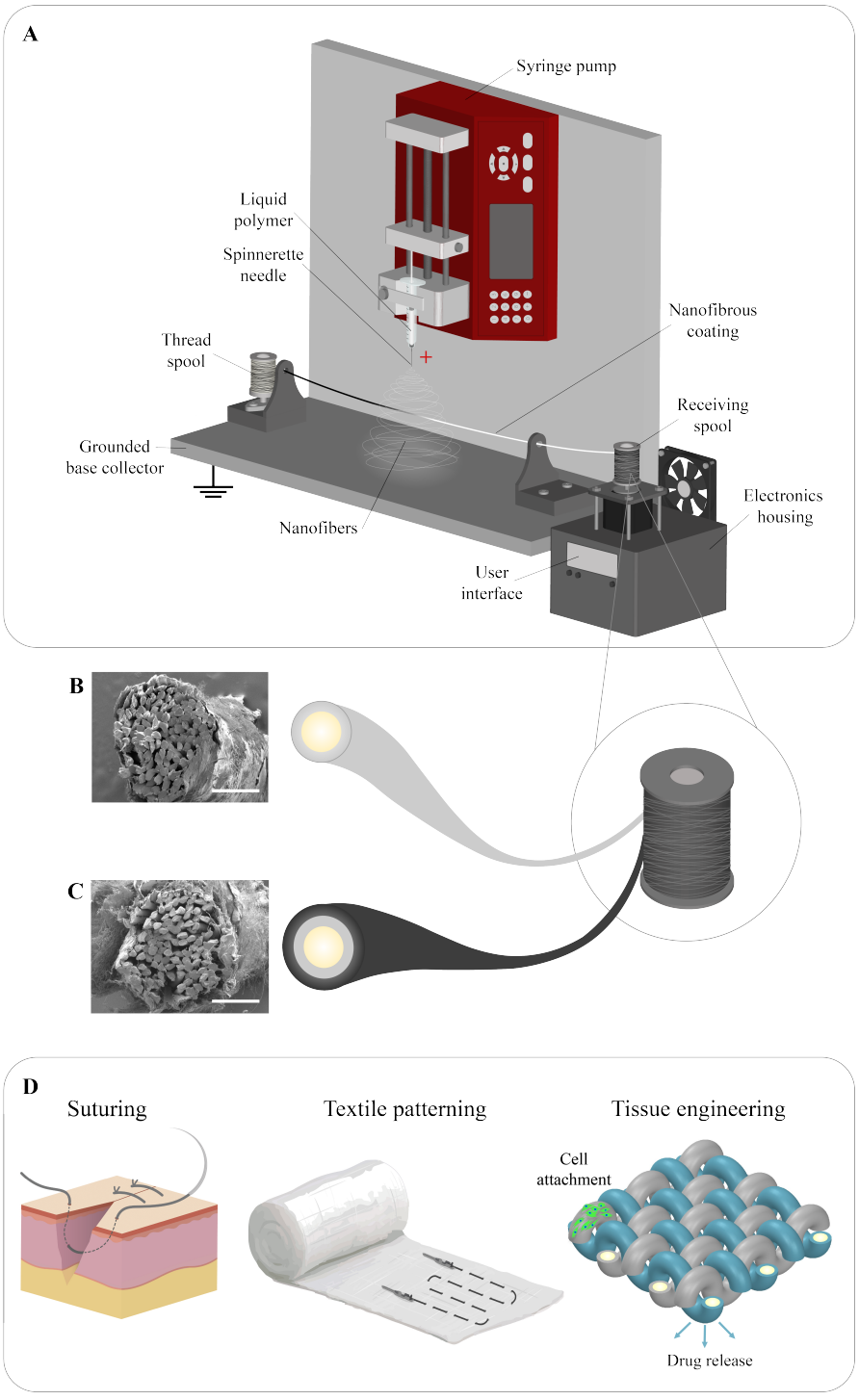

Figure 2.1: (A) Schematic of the proposed ES setup. A syringe pump, elevated above a base collector plate, is loaded with a syringe and needle containing polymer. Two spools opposite the area of nanofiber deposition move the thread from left to right, beneath the spinerette. Custom 3D printed housing for electronics, physical user interface, and microstepping motor is attached beside the collecting plate. (B) SEM cross-sectional image of single layer and (C) double layer coated thread (scale bars = 1.5mm). (D) Schematic illustration of electrospun coated thread applications: surgical sutures, wound dressing components, and scaffold materials for 3D tissue culture providing positive cell growth environment and drug/bioactives release.

2.2 Innovative components

Innovation is demonstrated in the following areas with the design of the proposed nanofibrous coating method:

- Allows for the fabrication of multi-layer coated thread constructs, utilizing polymers with different additives, chemical, and physical properties.
- Bench-top high-throughput (17.5mm of thread coated per second) manufacturing possible using an economical spooling mechanism and commercial controller.
- User-determined control over nanofibrous layer thickness and deposited fiber orientation with respect to the direction of the thread.
- Employs highly adaptable, cost-effective, and commercially available core structure threads/sutures for a wide range of applications.

2.3 Polymer optimization

The formability and morphology of electrospun fibers is dependant on the physical and chemical parameters of the given ES polymer solution. These parameters include viscosity, electrical conductivity, and polymer concentration. Low polymer

concentrations, low molecular weight, and poor solubility are characteristics of polymers which decreases the ES efficacy, where the solutions do not contain sufficient material to produce the stable and solid fibers. Huang et al. prove that higher solution viscosity results in the formation of thicker fibers with fewer bead irregularities occurring along the length of the nanofibers [70]. Solutions with low viscosity result in undesirable droplet formation, beaded nanofibers, and jet instability [71], as the fiber surface texture, morphology, and porosity are critical for biomedical applications. The topographical nanoscale fiber texture can provide cues for cellular attachment proliferation, and viability [72]. The porosity of the ES mat constructs, determined by the volatility of the solvent, effects total surface area which is important for biosensing and drug delivery applications [73].

PCL, a biodegradable synthetic polymer, has a history of regular use in medical applications [74]. The slow biodegradability characteristic and easy combination of PCL with other polymers for the formation of composites and co-polymers make it a desirable material for scaffolds used in tissue engineering, and a desirable material for surgical sutures and micro and nano drug delivery [75]. Hackett et al. demonstrated successful ES of 15 ww% PCL dissolved in 4:1 DCM (dichloromethane) and methanol [76]; parameters which were followed in this study.

Silk fibroin is a natural high molecular weight protein polymer that is produced by the silkworm species *Bombyx mori*, and is used extensively as a polymeric biomaterial for drug delivery [77]. Silk fibroin also exhibits beneficial properties such as high biocompatibility, biodegradability, aqueous processing, and the ability to form crystalline polymer matrices [78]. Researchers found that silk fibroin with a concentration of 13ww% in formic acid was demonstrated to be electro-spinnable at room temperature [79].

Gelatin is a highly biocompatible, bioactive, and hydrophilic biopolymer; proper-

ties which make it a promising scaffolding material for recapitulating the ECM [80]. The high biocompatibility and bioactivity of this natural polymer is caused by the existence of specific amino acid sequences; preferable sites for cell interactions [80]. The preparation of this material by use of ES methods results in a structure with a smooth surface and high surface area-to-volume ratio. Researchers Ki et al. electrospun 13% ww gelatin from porcine skin dissolved in formic acid into ultrafine fibers [81]. This ES polymer concentration and solvent formula was consequently followed in this study.

PNIPAm (Poly(N-isopropyl acrylamide) demonstrates thermo-responsive behavior at its LCST (lower critical solubility temperature) of 32°C in aqueous solutions, undergoing reversible phase transition in response to environmental temperature change [82]. Below 32°C, PNIPAm is hydrophilic; upon a temperature switch above 32°C, PNIPAm becomes hydrophobic and the rapid dehydration of the polymer network results in the release of encapsulated drug components. Additionally, PCL-PNIPAm blended polymers have been shown to generate electrospun fibers with high cell viability and cell alignment [83], and suppress the release of loaded drugs at higher temperatures [84]. PEGDA (polyethylene glycol diacrylate) is a photosensitive hydrogel, and has been used to elicit cell behaviors and adhesion, and has increased interest as a scaffolding material for biomedical applications [85]. The combination of PEGDA with secondary polymers (used as a viscosity modifier to facilitate fiber formation) has been demonstrated in literature [86, 87].

Among the family of conductive polymers, polymer PEDOT:PSS (poly (3,4- ethylenedioxythiophene):poly(styrenesulfonate) is a widely studied material used in flexible and portable electronics [88]. Notably, Bessaire et al. successfully demonstrate the usage of PEDOT:PSS for conformable conductive electrospun coatings for nonplanar surfaces [89]. The aqueous solution of PEDOT:PSS was combined with PEO

(poly(ethylene oxide)) with the addition of conductive DMF (dimethylformamide) as the ES solvent. PEO, a biocompatible and porous material, is widely used for applications involving tissue engineering scaffolds, and is soluble in aqueous solutions [90]. The ES parameters and polymer combination for conductive coated threads, discussed in Section 4.1, was optimized following the research by Bessaire et al.

Polymer concentration plays an important role in the viscosity of the ES solutions via intermolecular interactions. As stated, the concentrations of the various polymers in the following experiments were optimized based on literature review. Similarly, the choice of solvent used to dissolve the polymer was based on findings in literature. The choice of solvent can significantly alter the fiber surface morphology, due to the characteristics of conductivity, boiling point, and heat of vaporization [91]. The details of the ES parameters for the chosen coating materials are given in Table 2.1. While the influence of these process parameters and the individual polymer solutions have been investigated with known correlations, the morphology of the electrospun fibers was found to often differ slightly from the predictions in literature, indicating that there are yet more ES parameters that influence the electrospun fiber morphology. Interestingly, the relative humidity of the ES environment has been shown to impact the morphology and mechanical properties of nanofibers [92].

Table 2.1: ES parameters for electrospun coated threads types.

Polymer	Solvent	Voltage (kV)	Flow rate (mL/hr)	Thread displacement (cm)	Application(s)
PCL	4:1 DCM/Methanol	14	0.1	5	• Biocompatibility
PCL+MNPs	4:1 DCM/Methanol	13	0.12	5	• Magnetic threads
PCL/PNIPAm + drug/drug models	4:1 DCM/Methanol	15	0.05	8	• Temperature responsive drug release • Antibacterial suture coating
Silk Fibroin + drug models	Formic Acid	16	0.07	2	• Passive drug release • Cell attachment • Biocompatibility
Gelatin	Formic Acid	16	0.07	2	• Cell attachment • Biocompatibility
PEO/PEDOT:PSS	DMF	16	0.07	3	• Electrically conductive threads

The details of the ES parameters for tested and unused coating materials are given in Table 2.2. The described ES materials were not used due to low or high polymer solution viscosity, issues with the conductive material loading, and non-uniform/unwanted resulting nanofibrous morphology.

Table 2.2: ES polymers and parameters with negative experimental results.

Polymer	Solvent	Voltage (kV)	Flow rate (mL/hr)	Thread displacement (cm)	Results
15wv% PCL+ 0.05-0.25% rGO (reduced graphene oxide)	4:1 DCM/Methanol	14	0.1	5	• Uneven thread coating: droplet formation on thread surface • No visible Taylor cone formation • Infinite measured resistance
15wv% PCL+ 0.1-0.2% fMWCNTs	4:1 DCM/Methanol	14	0.1	5	• Poor fiber formation: droplets along thread surface • Visible clumping on thread surface • Infinite measured resistance
15wv% PNIPAAM (MW=135Da)	Methanol	12	0.15	3.5	• Electrospraying not ES: crystalline structures formed
5wv% PNIPAM (MW=300,000Da)	Methanol	13.5	0.15	3.5	• Flat, ribbon morphology fibers • 100% dissolved in H_2O
5wv% PCL/ PEDOT:PSS	DMF	16	0.07	5	• Poor solvent evaporation: merged NFs on thread surface

2.3.1 Electrospun fiber morphology

To determine the efficacy of the ES parameters with the various polymers, SEM images were taken of the ES fiber morphology. ES fiber morphology of the three main polymer materials in following experiments (PCL, gelatin, and silk fibroin) were examined, chosen to represent the flexibility of the developed fabrication method. In Figure 2.2, SEM images of gelatin, silk fibroin, and PCL nanofibers deposited onto the (stationary) curved thread surface. SEM images of electrospun coated sutures were acquired by a Hitachi electron microscope (Hitachi S4800, Tokyo, Japan) with 1.0 kV voltage to determine the structural features of the fabricated electrospun substrates. Samples were mounted on aluminum stubs using double sided tape, then coated with gold-palladium hummer sputter (Hummer VI sputter coater, Anatech USA, Hayward, CA, USA). The images show the differences in both fiber diameter and pore size of the resulting ES coating. The resulting fiber morphology of the three polymer coatings was found to be comparable to that of ES mats formed on flat base collectors [74, 79].

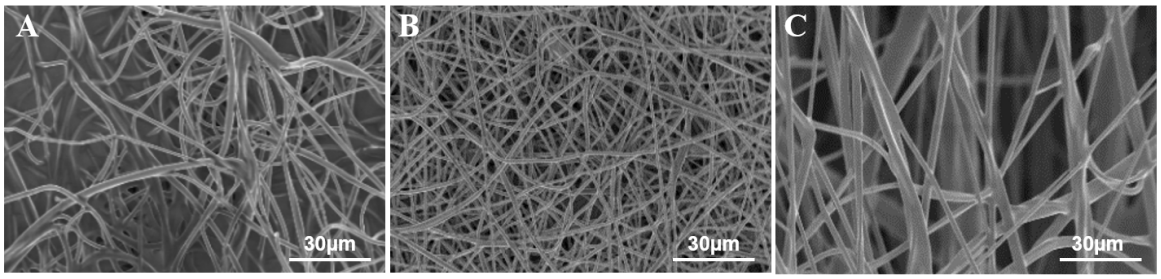

Figure 2.2: Electrospun fiber morphology. SEM images of electrospun (A) gelatin, (B) silk fibroin, and (C) PCL nanofibers on thread surface (spooling velocity = 0 mm/s, ES time = 30 sec).

2.3.2 Electrospun fiber diameter

The mean diameter and standard deviation of the fibers was measured from SEM and light microscope images for the ES polymers listed in Table 2.1. The fiber diameter was lowest for conductive PEDOT:PSS/PEO (1.226±0.45 μm), and increased for silk fibroin (1.381±0.37 μm), gelatin (1.43±0.24 μm), PCL (3.56±2.12 μm), PCL/MNPs (4.26±1.49 μm), and PCL/PNIPAm/PEGDA (10.65 ± 4.87 μm) (Figure 2.3). The standard deviation in the diameter measurements was used to determine if the chosen ES parameters resulted in uniform electrospun fibers. For PCL, PCL/PNIPAm, and PCL containing Fe_2O_3 MNPs, a larger fiber diameter and higher standard deviation in uniformity was seen when compared to gelatin and silk fibroin fibers. These findings were consistent with the common electrospun fiber diameters found in literature [74, 79, 81].

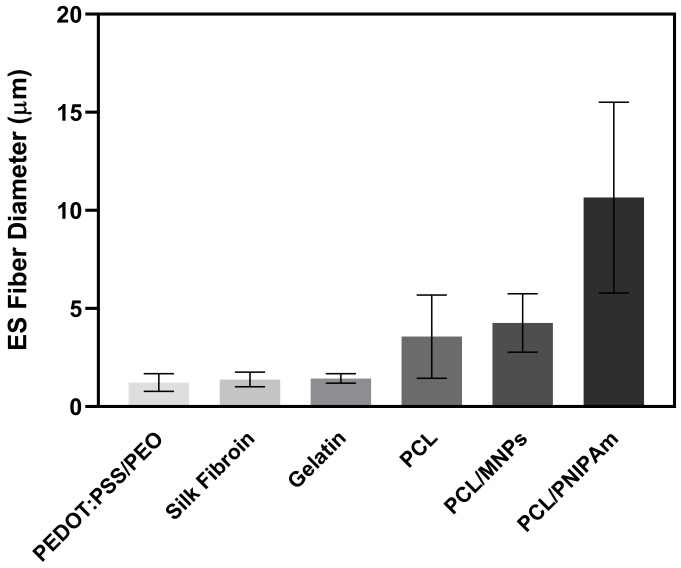

Figure 2.3: Fiber diameters of the studied ES polymers (n = 20, spooling velocity = 0 mm/s, ES time = 30 sec).

2.4 Thread fabrication

Section 2.4 outlines the materials and methods used to fabricate the electrospun coated thread and structure types used in the following experiments. A multifilament 100% nylon upholstery thread (Coats & Clark Inc., USA) was used as the basis for all coated thread types. This nylon thread material was chosen due to its resemblance with multifilament nylon suture material, a non-absorbable polymer suture commonly used in wound closure [93].

2.4.1 PCL coated threads

15 ww% PCL (MW 45,000, Sigma Aldrich, USA) was dissolved for ES in an 4:1 ratio of DCM (CH_2Cl_2, Sigma Aldrich, USA) and methanol (Fisher Chemical, USA. The solution was kept at constant agitation at room temperature for 2 hours until the solution became homogeneous.

2.4.2 Gelatin coated threads

13 ww% gelatin (300g Bloom, Type A, Sigma Aldrich, USA) was dissolved in formic acid (Sigma Aldrich, Saint Louis, USA) and kept at constant agitation at room temperature for 8 hours until the solution became homogeneous. The nanofibrous coated threads were crosslinked in glutaraldehyde (Grade 1, 25% solution in H_2O, Sigma Aldrich, USA) vapor. Briefly, 3 mL of glutaraldehyde solution and 100 μL of HCl (37%, Sigma Aldrich, USA) was added to 20 mL of dH_2O (distilled water) in a 10 cm petri dish. Gelatin coated threads were suspended above the petri dish within a sealed vacuum chamber for 6 hours, until a visible color change from white to yellow occurred. A final washing step to remove the glutaraldehyde residues was performed. Threads were gently agitated in 1% glycine (NH_2CH_2COOH, Sigma Aldrich, USA) in dH_2O for 10min, followed by 10min in dH_2O, repeated three times.

2.4.3 Silk fibroin coated threads

Silk cocoons from *Bombyx mori* were obtained from the Iranian Silkworm Research Center, and boiled in 0.02 M aqueous sodium carbonate (Na_2CO_3; 106392, Merck, Germany) solution for 1 hr to remove sericin, washed with dH_2O and dried at 37°C overnight. The degummed silk was then dissolved in 9.3 M Lithium Bromide (LiBr; 746479, Sigma-Aldrich, Saint Louis, USA) at 60°C for 4 hr, then dialyzed in a cellulose dialysis tube (12 kDa, Sigma Aldrich, Saint Louis, USA) against deionized water (diH_2O) for 72 hr. The silk solution was then lyophilized (MC4L, UNICRYO, Freeze-dryer, Germany) into prepared SF sponge [94], which was dissolved at 13 ww% for ES in formic acid under constant agitation for 8 hr. Electrospun silk fibroin was crosslinked by immersion in 70% Ethanol (Sigma Aldrich, USA) for 1-10 minutes.

2.4.4 Silk fibroin drug-loaded threads

Large molecule Fluorescein isothiocyanate-dextran (FITC-Dextran, MW = 40,000 Da, Sigma Aldrich, USA) and small molecule Rhodamine B (MW 500 Da, Sigma Aldrich, USA) fluorescent drug models were added to 100 μL of dH_2O and vortexed to dissolve. The aqueous solution was added to the silk fibroin solution at a concentration of 1 mg/mL fluorescent drug models and vortexed to combine.

2.4.5 Conductive threads

Electrically conductive threads were prepared based on research by Bessaire et al. [89]. Briefly, 0.134 g PEO (Polyethylene oxide, Sigma Aldrich, USA) was dissolved in 0.345 mL DMF and 2.56 g PEDOT:PSS PH1000 aqueous solution (Poly(3,4-ethylenedioxythiophene) polystyrene sulfonate, Ossila, UK) was combined at room temperature, under constant stirring for 24 hours. Electrical resistance was measured using a digital multimeter (Fluke 87 True RMS Multimeter, Fluke, Canada).

2.4.6 Magnetic threads

Magnetic functionalization of PCL ES solution was performed with the addition of 4 w% Iron (III) Oxide (Fe2O3, <50 nm particle size, Sigma Aldrich, USA) to prepared PCL ES solution (Section 2.4.1). Iron (III) Oxide powder was added to 15 wv% PCL solution and kept under constant agitation for 2 hours at room temperature. Aggregation of the MNPs in the ES polymer solution visibly occurred due to magnetic attraction. For even MNPs dispersal, the ES solution was ultrasonically mixed (Ultrasonic cleaner MH Series, Branson) for 2 minutes immediately prior to ES to ensure uniformly dispersal.

2.4.7 Temperature responsive drug releasing threads

10 wv% PCL was dissolved in a 4:1 ratio of DCM and methanol. 10 wv% PNIPAm (MW = 300,000 Da) was dissolved in a 4:1 ratio of DCM and methanol. The solutions were then combined and stirred until homogeneous at room temperature (1 hr). FITC-Dextran, Rhodamine, and doxycycline hydrochloride (MW = 444 Da, Sigma Aldrich, USA) were added separately to 100 μL of (dH_2O) and vortexed to dissolve. The fluorescent drug models were added to ES solutions at a concentration of 1 mg/mL. The aqueous solution containing antibiotic was added to an ES solution at a concentration of 1 mg/mL doxycycline hydrochloride. Electrospun coated samples were washed in dH_2O for 30 minutes at 200 RPM in a plate shaker (Titer Plate Shaker 120V, Thermo Scientific^{TM}, USA) to remove all excess unattached drug.

2.5 Feasibility study

Characteristics of the coated threads and the fabrication process were examined in a feasibility study to determine the effect of ES and fabrication method parameters. The coated threads were examined for coating layer thickness with respect to spooling velocity, distance between the horizontal thread and the tip of the spinerette needle, and total ES time (defined to be the period in which the voltage and electrical field is applied). In addition, the angle of the deposited electrospun fibers in the coating on the threads was examined. Based on the principles of the rotating drum ES method, ES onto a moving collector thread was hypothesized to align the electrospun fibers in generally uniaxially aligned arrays. The following sections demonstrate these changes on electrospun fibers and coatings with PCL concentration of 15 wv%.

2.5.1 Electrospun layer thickness

Figure 2.4 shows the change of electrospun layer thickness as a function of spooling speed. Layer thickness was measured from light microscope images of coated threads, subtracted by the diameter of plain threads. When spooling speed was increased from 0 mm/s (thread stationary under spinerette) to 17.5 mm/s, layer thickness decreased to approximately zero measurable thickness. At higher spooling velocities, the inability for nanofibers to deposit on the threads surface may be caused by turbulent air flow around the perimeter of the thread [95].

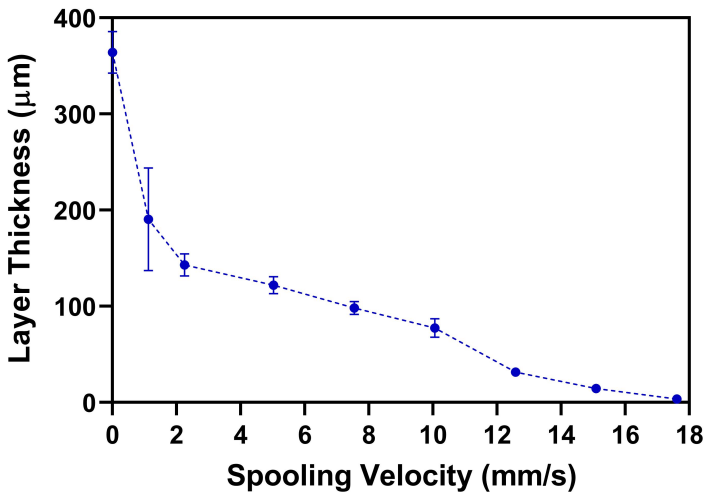

Figure 2.4: Electrospun layer thickness as a function of spooling speed (n = 3, thread-needle displacement = 5 cm).

Figure 2.5 shows the change in layer thickness as a function of spinning displacement for stationary threads. At the smallest displacement of 1 cm, layer thickness is lowest (25.42 ± 10.17 μm). When the spinning distance is widened to 6 cm, the electrospun coating thickness increases to a maximal value of 76.80 ± 5.55 μm, then sharply decreases at 7 cm and 8 cm displacement. This initial increase in thickness may be due to the morphology change of electrospun fibers from flat to cylindrical morphology, with increased space between the consecutively deposited cylindrical fibers. Flat

electrospun fibers may occur at decreased displacements as the wet (non-evaporated solvent) fibers collide with the thread, changing from cylindrical to flat fibers on impact [96]. The electrospun helical jet thins, stretches, and solidifies at largest distances from the spinneret [97]. The lower layer thickness at the largest thread-needle displacement (8 cm) may be due to this stage of jet formation and thinning, where there is greater dispersal of fibers [96].

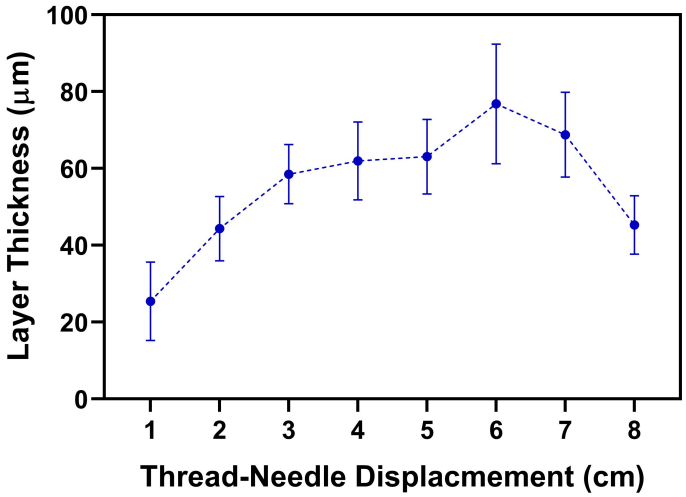

Figure 2.5: Layer thickness as a function of spinning distance (n = 3, spooling velocity = 0 mm/s, ES time = 60 sec).

Figure 2.6 shows the resulting electrospun PCL layer thickness on stationary threads as a function of total ES time, or the time during which an electric field acts upon the liquid polymer drop at the spinerette needle. With increased total ES time, layer thickness increases approximately linearly. This was an expected finding, as the diameter and rate of fiber fabrication can be considered approximately uniform during the period that the electric field is applied. With increasing time, the number of electrospun fibers that are deposited onto the surface of the thread increases, accumulating in stacked layered meshes, thus increasing the layer thickness. Similarly, when ES PCL onto a flat collector plate, researchers found that longer production

times increased the fiber deposition density, resulting in increased fiber mesh apparent thickness [98].

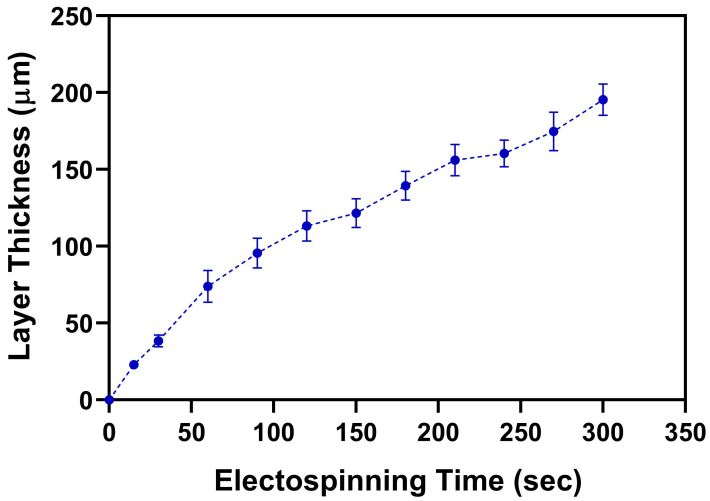

Figure 2.6: Layer thickness as a function of total ES time (n = 3, spooling velocity = 0 mm/, thread-needle displacement = 5 cm).

2.5.2 Electrospun fiber orientation

The use of a rotating conductive collector (i.e. mandrel, wire drum, cone, wheel, or frame form) in an ES setup was the earliest method used to fabricate aligned nanofibers [99]. The rotating drum collector, which is oriented perpendicular to the needle spinerette, was developed by Matthews et al. to collect aligned electrospun fibers. With control over the rotation speed of the drum collector, fiber alignment increased with rotational drum speed, up to a maximal velocity of 12.9 m/s [100]. Furthermore, researchers reported that the optimal orientation of electrospun fibers occurs when the linear velocity of the rotating cylindrical drum matches the speed of the evaporating jet depositions [100, 101]. With this method, fibers are deposited onto the surface of the drum in a circumferential manner due to the high velocities and/or the imparted mechanical stretching forces. This velocity-dependant fiber alignment

does not occur when the rotating velocity is too low to initiate fiber orientation or if extreme rotating velocity causes turbulent air flow around the perimeter of the rotating collector but will be induced at a threshold speed. The threshold speed for fiber alignment has been found to vary system-to-system [95].

Based on the principles of the rotating drum ES method, electrospun fiber deposition onto a moving collector thread were hypothesized to align in generally uniaxially aligned arrays. Figure 2.7 shows the trend of the angle of deposited electrospun fibers on the surface of the thread, with respect to the direction of the thread. At lower velocities (1-10 mm/s), a high standard deviation in fiber orientation indicates the random and unaligned nature of the deposited fibers. At higher velocities (12.5-17.5 mm/s), fiber angle approaches zero and standard deviation decreases to ±10°, demonstrating alignment of fibers along the length of the thread. Based on the results from Section 2.5.1, the layer thickness of these aligned fibers would also be reduced.

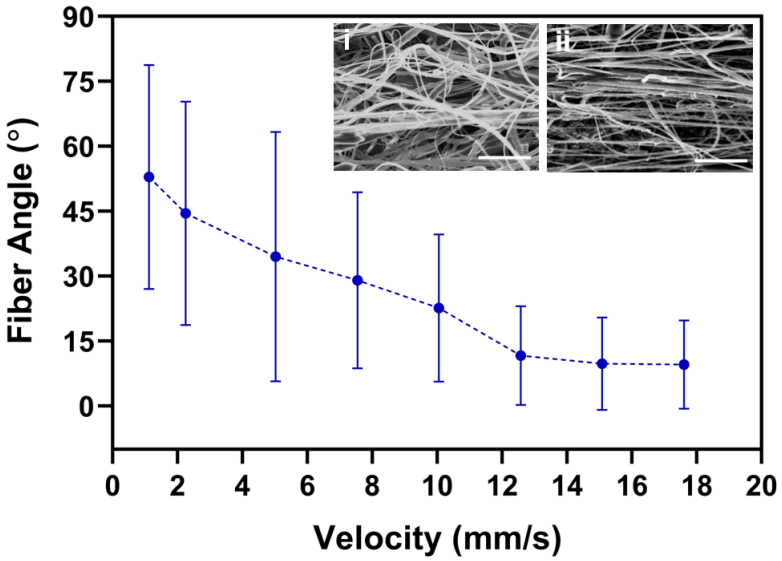

Figure 2.7: Absolute angle (relative to the direction of the thread) of deposited electrospun fibers on the surface of the thread (n = 100, thread-needle displacement = 5 cm). Inset SEM images of (i) deposited fibers at 1 mm/s spooling speed and (ii) 17.5 mm/s spooling speed.

The frequency distributions of the deposited electrospun fiber orientation for 1 mm/s and 17.5 mm/s spooling speeds is shown in Figure 2.8A and B, respectively. At the highest spooling speed, a Gaussian distribution (R = 0.9655) is seen, while there is a random distribution as lower spooling speeds. These findings indicate that fiber orientation is random with respect to the direction of the thread at low spooling velocities.

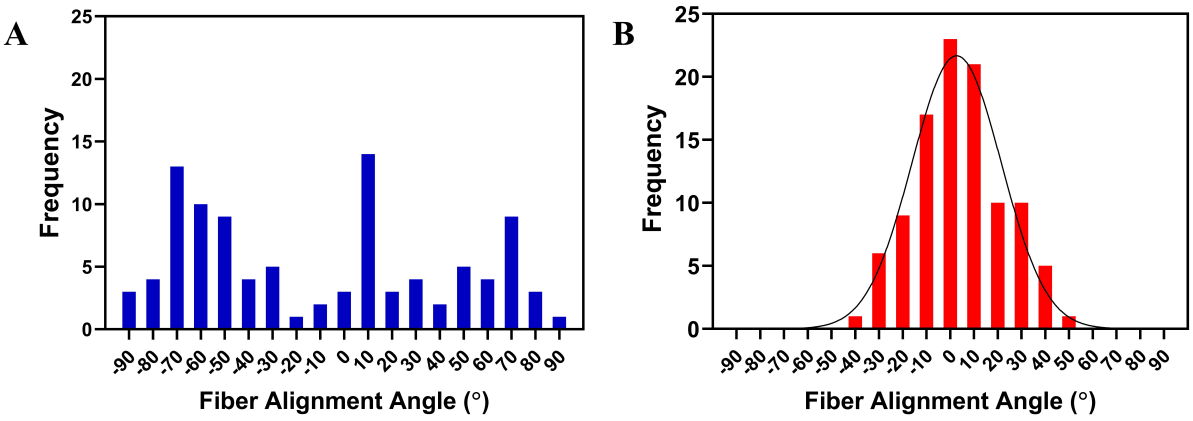

Figure 2.8: Frequency distribution of the measured angles for (A) 1 mm/s and (B) 17.5 mm/s spooling speeds.

2.5.3 Electrospun coating lamination

Given the intended suture application requires drawing of the thread through tissues, the potential for PCL coatings to delaminate from the base thread substrate was studied. Tested in triplicate, a 1.5 cm long PCL coated thread was fabricated as per Section 2.4.1; a 4 mm section was left uncoated by applying masking tape to one end of the thread during the ES process. The tape was then removed following the ES process, and the uncoated end of the thread was glued (Gel Control Super Glue, LePage) to the inner lid of an Eppendorf Tube (1.5 mL, Eppendorf) containing 1.5 mL dH_2O (Figure 2.9). The thread samples were suspended on the surface of

the water and were subsequently centrifuged at 6000 RPM for 15, 30, 60, 120, and 900 seconds. In this method, centripetal force was applied and acted on the coating material solely, while the thread core was fixed. The results of this experiment showed that there were zero instances of visible electrospun layer delamination for triplicate thread samples for up to 15 minutes duration of centrifugation.

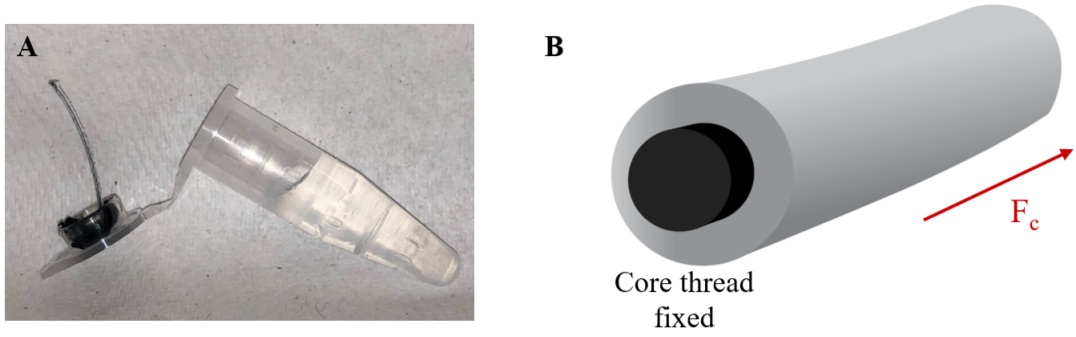

Figure 2.9: (A) Delamination test setup. (B) Schematic of force acting only on the electrospun thread coating.

2.6 Thread mechanical strength

The stress-strain response of PCL coated threads was investigated for future work in the application area of stress-strain sensors for biomedical applications. PCL coated threads were chosen for tensile testing as the coating process is fast (due to the large fiber diameter) and as this polymer requires no post-ES crosslinking procedures. While only one polymer was chosen for the mechanical analysis for proof-of-concept purposes, different ES polymer coatings may be assumed to alter the tensile strength results of coated threads, depending on the inherent mechanical properties of the coating material. These findings are intended to showcase a preliminary proof-of-principle.

2.6.1 Mechanical testing setup

Mechanical testing was performed using a tensile tester (MTI-10K, Measurements Technology Inc., USA). Custom machined metal clamps were attached to the two ends of thread samples, overlapping with the electrospun coating on both ends. The clamped thread samples were loaded into the tensile testing apparatus with slack, so that the samples did not experience premature loading. All thread samples were stretched at a crosshead speed of 3 mm/min from the initial length of 3 cm (gauge length). Young's modulus and elongation at break were derived from the generated force versus displacement curves.

2.6.2 Tensile experiment results

The displacement of the uncoated and PCL coated threads with applied load is shown in Figure 2.10A. The displacement of coated threads with applied load was higher than that of uncoated threads, with a difference of around 85.3 μm. Figure 2.10B shows the stress-strain plot of plain threads compared to threads coated in electrospun PCL. The lower ultimate tensile strength and elastic modulus in the PCL-coated threads may be due to the 85.6% increase in the cross-sectional area of the coated threads to uncoated threads. The average area for uncoated threads is 0.072 mm^2, with an additional area of 0.133 mm^2 upon coating. In addition, stress shielding of the electrospun coating by the core thread may have occurred due to the difference in elastic moduli of the core nylon thread and electrospun PCL nanofibers with DCM/methanol solvent (6.812 ± 0.301 MPa and 3.5 ± 1.1 MPa, respectively [76]).

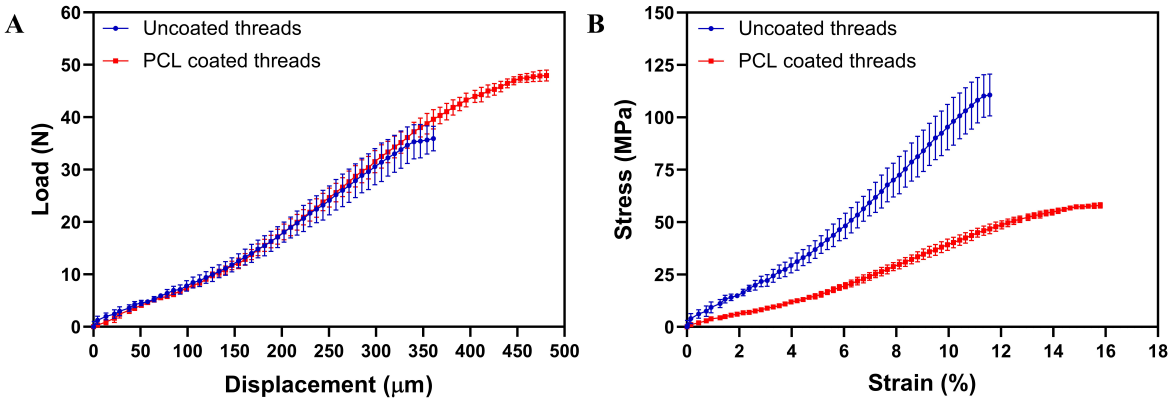

Figure 2.10: (A) Load versus displacement of uncoated threads and PCL coated threads. (B) Stress-strain plot of plain core threads and PCL coated threads (n = 3, spooling velocity = 3 mm/s, thread-needle displacement = 5 cm).

Electrospun coated threads demonstrated significantly longer elongation relative to their original length (Figure 2.11A) when compared to uncoated threads ($15.5 \pm 0.43\%$, $13.4 \pm 0.66\%$, respectively). However, the Young's Modulus of *in vivo* human skin has been experimentally found to be between 0.42 and 0.85 MPa [102, 103], nearer to that of the PCL coated threads compared to uncoated threads (3.80 ± 0.21 MPa and 6.81 ± 0.30 MPa, respectively), shown in Figure 2.11B. Were these coated threads used as suturing materials, the higher degree of elasticity would provide clinical advantages. The coated threads are less likely to cut through the skin with swelling while effectively approximating wound edges during the healing process by returning to the original length after swelling has subsided [104].

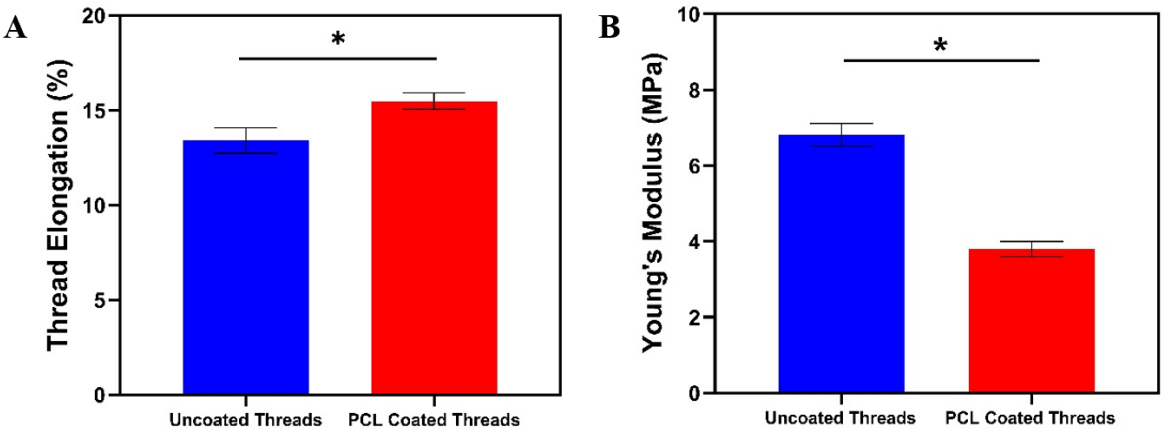

Figure 2.11: (A) Percentage of thread elongation of plain threads and PCL coated threads. (B) Young's Modulus of plain threads and PCL coated threads ($p* < 0.05$, n = 3).

2.7 Statistical analysis

Results were analyzed by GraphPad Prism Version 8 (GraphPad Software, CA, USA). Statistical significance was analyzed using unpaired parametric t-test for two independent samples, not assuming equal deviations. Experimental results were done in biological replicate (n = 3). The preliminary conductive thread temperature response experiments in Section 4.1.1 were completed with single replicate (n = 1). Mean and standard deviation reported. P value reporting is as follows: $p* < 0.05$, $p** < 0.01$, $p** < 0.001$, $p* * ** < 0.0001$.

Chapter 3

Multifunctional thread assembly using textile methods

The proposed electrospun coated threads can be successfully manipulated with different fabrication methods, in addition to being used as sutures in skin models. The versatility of the nanofibrous coated threads is demonstrated in the following Sections, and SEM images of the constructs show the coating fiber morphology after textile manipulation. The assembly of these coated threads into 1D-3D structures by braiding and weaving methods supports their use as potential scaffolds for tissue engineering applications. Textile fabrication technologies enable the threads to be engineered into structures with the required properties for various biomedical applications [105]. For example, embroidery, weaving, knitting, and braiding have been used to fabricate scaffold constructs for applications in tissue types such as cardiac [26], skeletal [47], skin tissue [24], and cartilage [106].

3.1 Braiding, weaving & knitting

1D structures such as braids have been studied for their cell-aligning capabilities, an important characteristic for tissue types with specifically orientated cells. The matrix patterning of ECM and cells in tissue types and organs such as corneal stroma, smooth muscle cells, tendon, bones, and skeletal muscles, are important for their function and efficacy [61]. The interaction between cells and the ECM are many, and remodelling of the ECM by cells is driven by different stimuli to generate these specific patterns. Additionally, braided textiles demonstrate high flexibility and structural stability, and are beneficial for load bearing engineered tissues such as tendon and bone [107]. Figure 3.1A shows a 1D braided structure of two electrospun coated threads with a plain nylon thread. The colorized SEM image shows the surface morphology of the threads coated in electrospun fibers (Figure 3.1A(ii)). The green fluorescent coating is loaded with FITC-Dextran and is comprised of silk fibroin, representing a thread that could carry large-molecule hydrophilic and macromolecular compounds such as growth factor proteins, for tissue engineering applications. The red fluorescent coating is loaded with Rhodamine and is comprised of PCL/PNIPAm, representing a thread that carries a small drug model, such as the antibiotic doxycycline, a promising therapeutic for chronic wounds [108].

Construction of 3D textile-based scaffolds allow for biomimetic cell culture, in comparison to 2D (two-dimensional) cell cultures [109]. Knitting textiles have high flexibility and allow for the creation of 3D complex structures [107]. The proposed fabrication method allows for high scalability of thread lengths, thereby allowing for further large-scale constructs. Fluorescent FITC-Dextran and Rhodamine were loaded in the multi-thread assemblies, demonstrating the multi-drug loading capabilities of the structures. Figure 3.1B shows a knit slip knot structure fabricated from an nanofibrous coated thread.

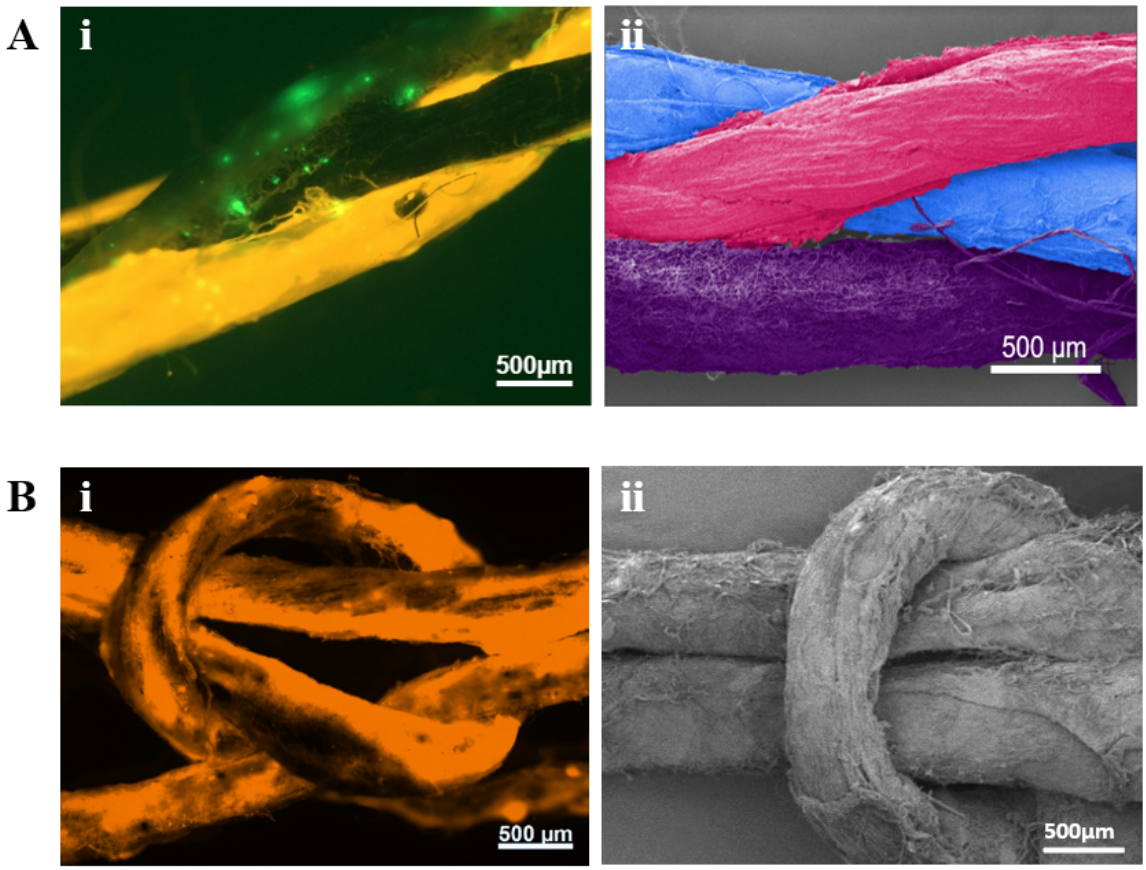

Figure 3.1: (A) (i) Braided structure with hydrophilic, hydrophobic, and plain threads, (ii) SEM image of surface texture in braided textiles. (B) (i) Knitted hydrophobic threads, (ii) SEM image of surface texture on knit structure.

Figure 3.2A shows a loom-woven structure with a hydrophobic PCL coated thread incorporated with plain hydrophilic cotton threads (shown in grey), while Figure 3.2B shows a woven structure fabricated with silk (green) and PCL/PNIPAm (red) nanofibrous coated threads. The green and orange fluorescent drug model-loaded threads are hydrophilic and hydrophobic, respectively. The ability to combine threads into structures with these differing wicking properties is beneficial, specifically in situations where wound exudate or blood may be drawn along the hydrophilic length of thread via wicking for biosensor applications [22]. Woven textiles also allow for constructs with anisotropic properties, and the process is less mechanically harsh

compared to knitted textile applications [107].

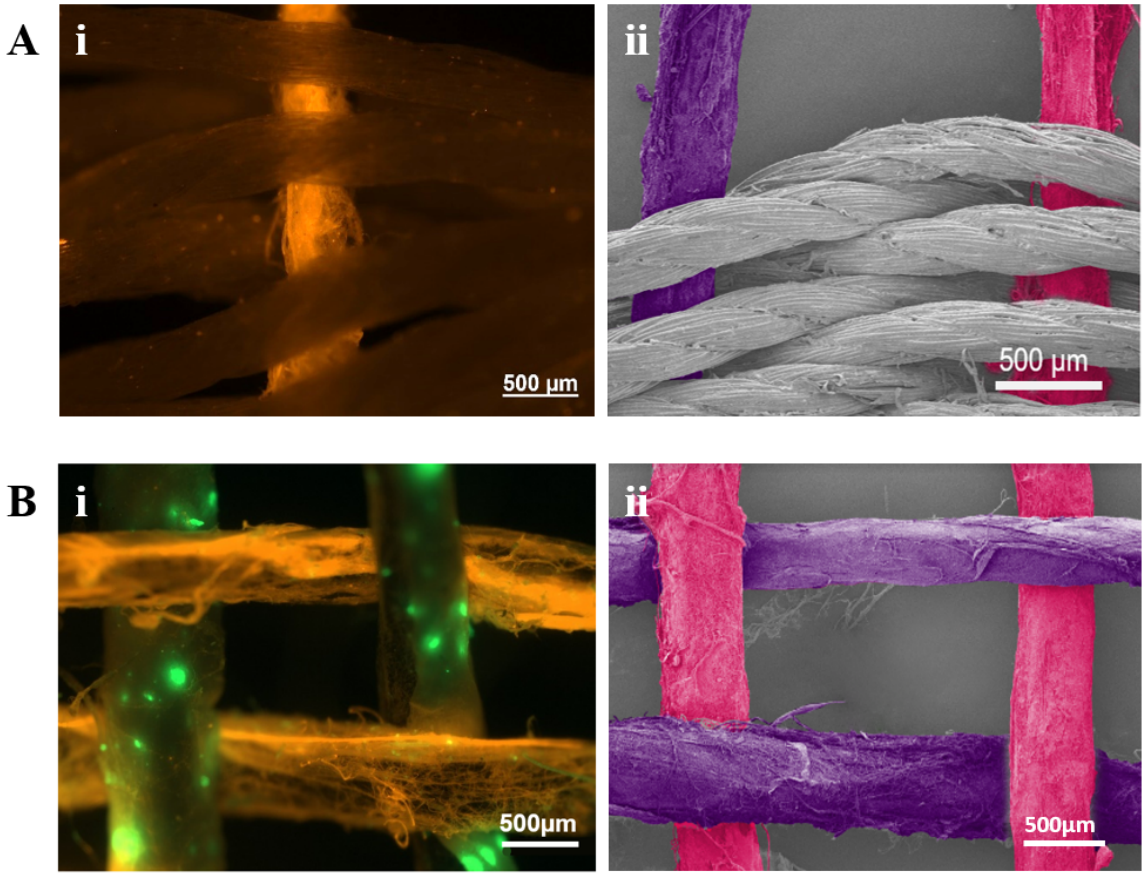

Figure 3.2: (A) (i) Loom-woven hydrophobic threads with uncoated plain threads, (ii) SEM image of surface texture on woven textiles. (B) (i) Loom-woven hydrophilic and hydrophobic threads, (ii) SEM image of combined woven structure.

3.2 Embroidery

Figure 3.3 shows a silk fibroin coated thread (white) sewn into cotton (grey) fabric. The SEM image (Figure 3.3(ii)) shows the surface morphology of the thread (highlighted in pink) once embroidered into the individual threads of the fabric. Embroidery of hydrophilic electrospun coated threads into fabrics can serve as microfluidic channels for the controlled delivery of wound exudate, blood, sweat, and tears in biological sensors, as demonstrated by Mostafalu et al. [22]. The use of sewn conductive

ES polymer coated threads may also have applications in textile-based wearable soft electronics.

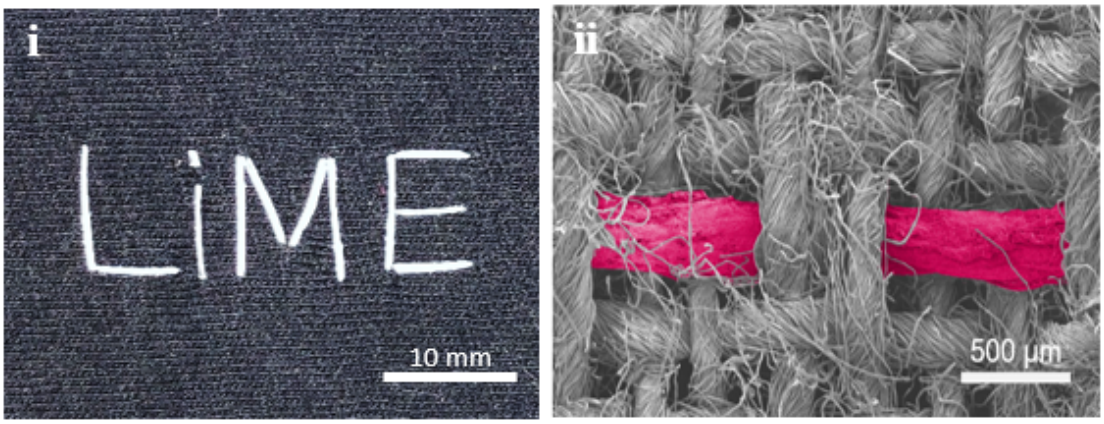

Figure 3.3: (i) Coated threads sewn into fabric, (ii) SEM image of sewn construct.

3.3 Suturing

The assortment of natural and synthetic coating materials can be leveraged to accommodate diverse wound types and the different stages of the wound healing process. An ideal nanofibrous coated suture material would promote tissue repair with minimal inconvenience and irritation for patients. This important application of these coated threads as suture materials is demonstrated in Figure 3.4. An *ex vivo* porcine skin model was used as a tissue model for human skin, due to the similarities in anatomy, and physiology, cellular composition, immunogenicity, and morphology [110]. An open wound was simulated by creating a 2 cm-long and 1 cm-deep incision in the skin model with a scalpel. Two standard two-handed square suture knots were placed into the incision with PCL nanofibrous coated threads acting as the suture material, which effectively approximated the tissues.

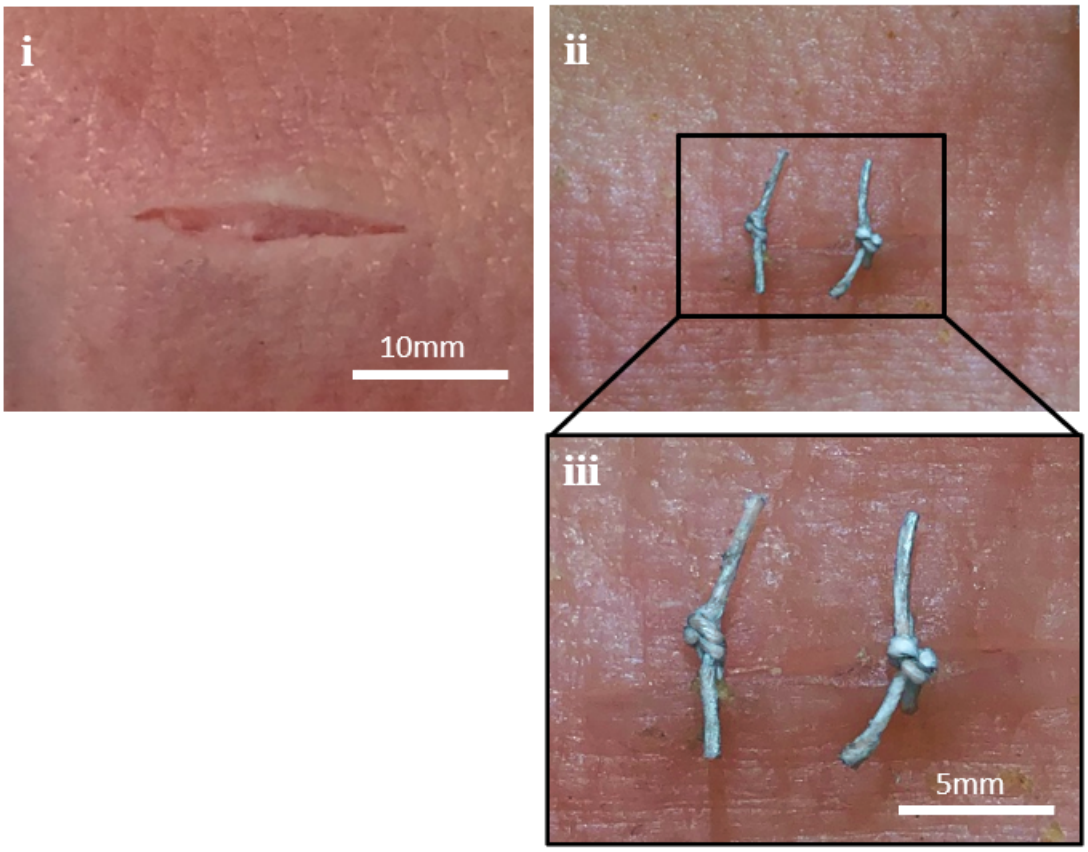

Figure 3.4: (i) Simulated open wound incision in pig skin. (ii) Incisional wound closed with two coated sutures, (iii) 2x magnified.

Chapter 4

Stimuli-responsive threads

In this study, electrospun coated stimuli-responsive thread-based structures were fabricated with ES polymers that respond to environmental changes. The application area of these threads is in wound bed or deep tissue environments, where increased localized wound temperature is a classic characterization of wound infection. A study by Dini et al. concluded that the qualitative wound bed temperature measurement is a reliable method for optimizing the assessment and diagnosis of chronic wounds health status [111]. The maximum temperature differential between wounds and healthy skin is +4-5.5°C with clinically diagnosed wound infection, and +1.5-2.2°C with clinical inflammation [112].

Additionally, these stimuli-responsive threads have applications in induced magnetic field stimulus and relative humidity (RH) monitoring of wound exudates. Wound exudate is produced during the inflammatory and proliferative healing stages, and the level can be an indicator of the status of the wound [113]; high moisture levels can be due to untreated underlying pathology or increased bioburden.

4.1 Conductive threads

For electrically conductive applications, threads were functionalized with PEDOT:PSS/PEO electrospun coatings as described in Section 2.4.5. A conductive coated thread (length of 2 cm) was used as a wire between a power source (5 V) and ground, as seen in Figure 4.1. The thread successfully acted as a conductor, allowing an in-series LED (light emitting diode) to be powered and lit, demonstrating the electrical conductivity of the length of the coated thread. The mean resistance of the conductive threads was measured to be 55 ± 23 kΩcm^{-1} at ambient temperature (23°C). The average conductive electrospun layer thickness was found to be 68.11 ± 7.19 μm.

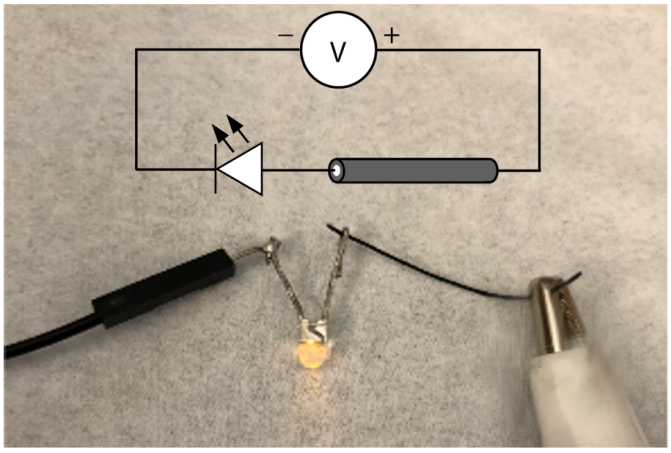

Figure 4.1: Electrically conductive thread (grey bar in inset circuit diagram) functions as a wire between power and ground, completing the circuit to light an in-series LED.

4.1.1 Resistive temperature response

Flexible temperature sensors can be categorized into three main types: pyroelectric detectors, resistive temperature detectors (RTDs), and thermistors. Thermistors rely on the thermo-resistive effect of a sensing material, and are widely used due to the simple device structure, fast response, and wide temperature sensing range [114].

The conductive PEDOT polymer exhibits temperature-dependant resistance changing characteristics, or thermistor behavior [115], and has been proven as a promising candidate due to the characteristic temperature and resistivity of PEDOT:PSS thin films having an inversely proportional relationship [114, 115, 116].

In a preliminary test, the PEDOT:PSS/PEO electrospun coated threads demonstrated an inverse change in resistance with applied heat, as shown in Figure 4.2. An environmental chamber (Model 123H, TestEquity, California, USA) was used to set thermal soak and ramp times. A 1 cm-long thread sample was placed in the environmental chamber programmed to change temperature from 20-50°C, with ramp temperature and time of 10°C/15 min, temperature soak time of 15 min, and RH of 30%. The electrical resistance of the thread was measured using a digital multimeter attached to the two ends of the thread via clamps. The measured resistance of the sample showed a sensitive response (approximately 70% change in resistance) to dynamically increasing temperature (change of 30°C) over a 75 minute duration.

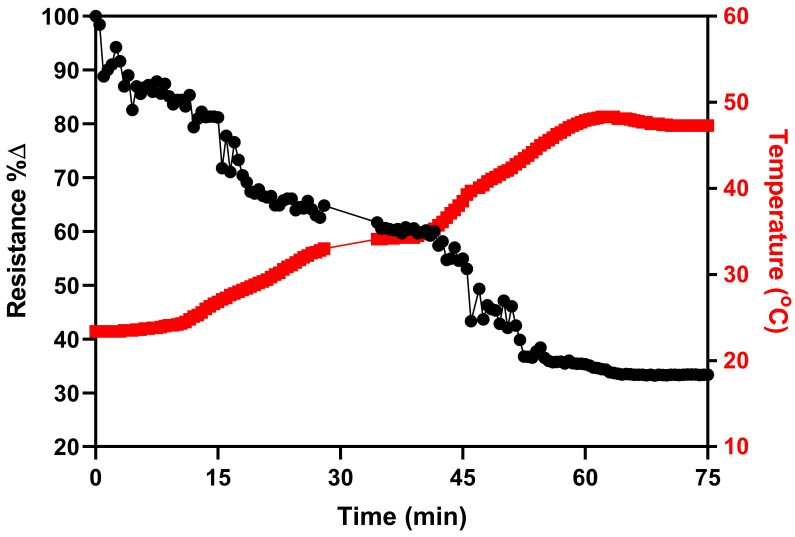

Figure 4.2: Resistive temperature response of electrospun conductive coated threads (n = 1, spooling velocity = 0 mm/s, ES time = 60 sec, thread-needle displacement = 3 cm).

The extended response of conductive electrospun coated threads at low (Figure 4.3A) and high (Figure 4.3B) physiologically relevant temperatures was characterized at RH 30%. Over a 30 minute period, the resistance response of the thread was captured and appeared approximately constant for both temperature conditions. At 20°C, a maximal 11% change from the starting resistance measurement as observed. Comparatively, at the higher 50°C constant temperature, change in measured resistance varied by only 5%. This preliminary study indicates that the resistance of the threads does not change considerably in consistent temperature conditions. A clear difference of 15.53% in average measured steady response resistance was observed between the high and low temperature conditions.

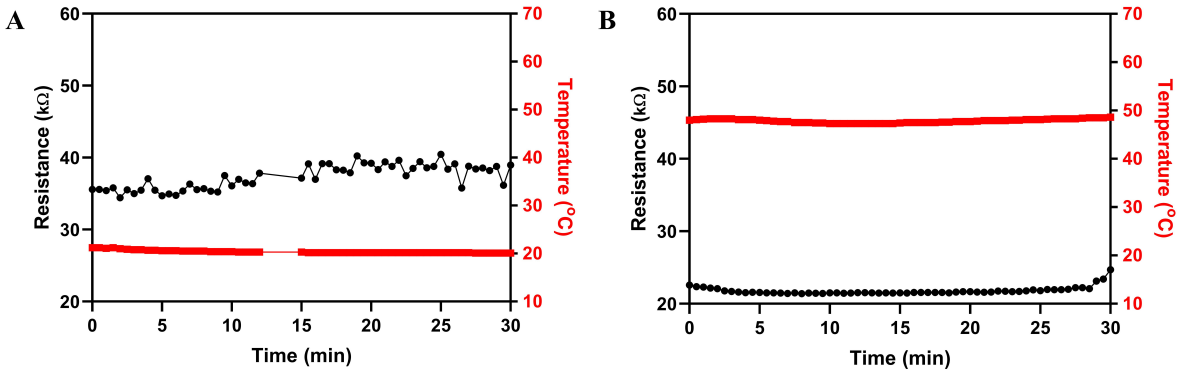

Figure 4.3: Steady resistance response for constant temperatures (A) 20°C and (B) 50°C (n = 1, spooling velocity = 0 mm/s, ES time = 60 sec, thread-needle displacement = 3 cm).

As PEDOT:PSS is a water soluble polymer, its use as a biological sensor with potential exposure to RH can cause unwanted cross-talk with temperature [117]. A preliminary test of the conductive coated thread response to environmental humidity conditions was performed. DiH_2O was sprayed onto the surface of a thread, connected via alligator clips to a multimeter for continuous resistance measurement. A measured $8.572 \pm 6.516\%$ decrease in resistance occurred within one second of the diH_2O ap-

plication (Figure 4.4). This immediate RH response was seen in triplicate samples, indicating that an RH-sensitivity exists for the as-ES conductive material on thread surfaces. However, the resistance response 30 seconds post-spray varied between samples, showing that the sensors may not return to their original resistance uniformly. This preliminary finding demonstrates the need for further study to develop the electrospun PEDOT:PSS/PEO based thread into a facile fabricated humidity-resistant temperature sensor.

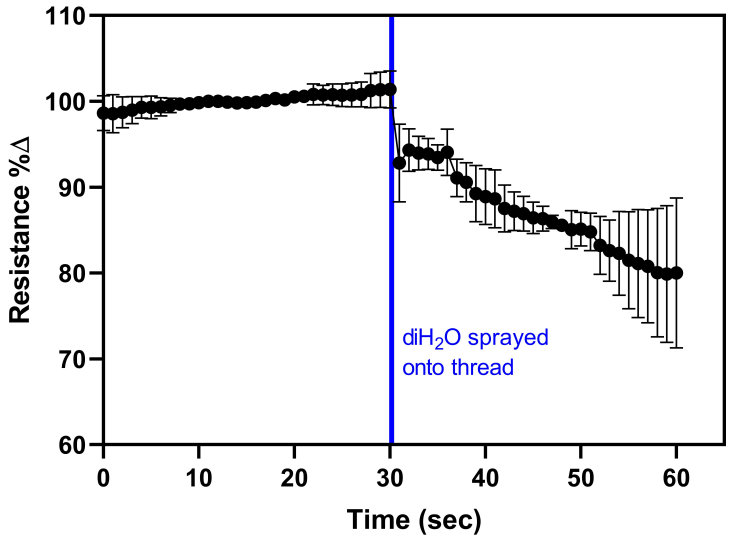

Figure 4.4: Characterization of resistive RH% response of conductive coated threads (n = 3, spooling velocity = 0 mm/s, ES time = 60 sec, thread-needle displacement = 3 cm).

4.2 Magnetic threads

Magnetic functionalized threads were coated in ES PCL containing dispersed Fe_2O_3 MNPs. Maghemite (λ-Fe_2O_3) is a common superparamagnetic iron oxide used in biomedicine due to its low toxicity, high rate of magnetization at room temperatures, and ease of functionalization [118]. Other metallic materials with high magnetic

moments such as cobalt and nickel, are toxic and prone to oxidation, which limits their application in biomedical fields [118]. Further, iron-based MNPs are highly biocompatible and the iron excess is efficiently degraded and removed by the body due to the well controlled iron-cell homeostasis or phagocytosis, depending on the MNP size [119]. MNP's and magnetic functionalization of scaffolds have important roles in drug release and tissue engineering. Areas of application include targeted drug delivery [120], tissue stimulation [121, 122], and hyperthermia [123, 124].

A 5 cm-long piece of thread was ES-coated, and a 1 cm diameter magnet was placed in the vicinity of the thread. As seen in Figure 4.5, the Fe_2O_3-containing thread coating was attracted by the magnetic field, resulting in the thread being lifted from the original resting position.

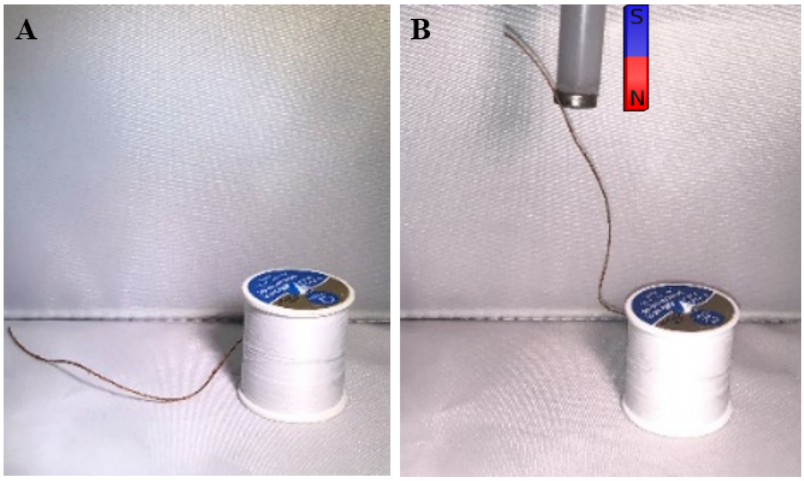

Figure 4.5: Coated magnetic thread (A) lying prone, (B) acted upon by a magnetic field and lifted from the original position (spooling velocity = 2 mm/s, thread-needle displacement = 6 cm).

Chapter 5

Thread-based drug release

The consecutive stages of wound healing are orchestrated by different cell populations such as neutrophils, macrophages, and fibroblasts, and molecular mechanisms of wound repair such as ECM proteins, peptide growth factors, and hormones [11]. If the wound healing response is impaired, a wound can become chronically non-healing, with excessive levels of proinflammatory cytokines, a deficiency of stem cells, and the existence of persistent infection and drug-resistant microbial biofilms [13]. The administration of oral or injectable antibiotics is the clinical standard of care, however systemic drug exposure may not be the optimal method of treating local wound complications [13]. Technologies such as drug-loaded sutures with localized delivery are an alternate solution, which overcomes negative effects such as drug-resistant microorganisms and systemic toxicity [125].

5.1 Passive drug release

For the application of drug release into the wound environment from implanted sutures, the passive release of a drug-model from coated threads was studied. Out of the studied polymers, silk fibroin polymer was chosen for passive drug release

from electrospun fibers due to its mechanism of crosslinking. The structure of as-spun silk fibroin fibers consists of α-helix and random coil components. However, the use of as-spun silk fibroin is limited because of the poor mechanical properties and poor water resistance due to the secondary structure [126]. With the introduction of post-processing crosslinking via aqueous organic solvent mixtures (immersion in 70% ethanol), silk undergoes a conformation change that results in a significant increase in β-sheet components, dependent upon the alcohol concentration and immersion time [126].

5.1.1 Degradation of silk fibroin

Silk fibroin coated threads were prepared (spooling velocity = 5mm/s, thread-needle distance = 2 cm), cut into 3 cm lengths, and crosslinked for 10 minutes in ethanol (70%). Samples were weighed at the beginning the experiment for the initial dry mass. PECF was used as simulated wound fluid exudate for the degradation measurements. Briefly, PECF (pseudo-extracellular fluid; $pH = 8.0 \pm 0.5$) was prepared by dissolving NaCl (Sodium chloride, 0.68 g), KCl (Potassium chloride, 0.22 g), $NaHCO_3$ (Sodium bicarbonate, 2.5 g), and NaH_2PO_4 (Monosodium phosphate, 0.35 g) in 100 mL of dH_2O [127, 128]. Threads were then placed in 1 mL of PECF and kept at 37°C (body temperature) for 18 days. The threads were periodically removed from solution and weighed for wet mass, then air dried and weighed for dry mass. Degradation percentage was calculated using Eq. 5.1, where M_i is the initial weight and M_D is the dry weight after degradation:

$$DR\% = \frac{M_i - M_D}{M_i} \times 100 \tag{5.1}$$

The wet to dry ratio of the coated thread samples was calculated using Eq. 5.2, where M_w is the wet weight after degradation:

$$Wet/Dry\ weight\ ratio = \frac{M_{\mathrm{W}}}{M_{\mathrm{D}}} \tag{5.2}$$

Figure 5.1 shows the degradation rate of silk fibroin coated threads in PECF medium over the 18-day period. Total sample mass degradation of the silk fibroin coating reached 6.06% over a period of 3 weeks. Additionally, the wet to dry ratio at 24hr was 1.217 and decreases approximately linearly towards 1 after immersion of the samples in the PECF for all subsequent time points, indicating that the PECF solution accumulation in the silk fibroin fibrous scaffold decreases over time.

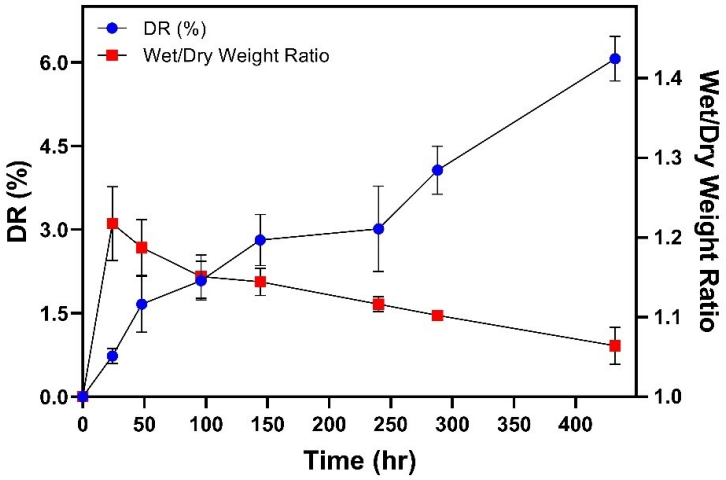

Figure 5.1: Degradation of silk fibroin thread coatings in PECF over 18 days (n = 3).

5.1.2 Crosslinking & release rate

Silk fibroin is susceptible to biological degradation by proteolytic enzymes which were not represented in the previous experiment, which limits the applicability of this study. The slow rate of degradation of silk fibroin that occurs in aqueous solutions instead relies upon hydrolysis under physiological pH, temperature, and osmotic pressure (130). The rate of FITC-Dextran release into PECF medium of silk fibroin coated

thread degredation was studied for three different crosslinking times (defined as the total time of thread immersion in 70% ethanol). FITC-Dextran loaded silk fibroin samples ethanol crosslinking solutions were reserved for fluorescent imaging. Samples were then washed in dH_2O for 30 minutes at 200 RPM in a plate shaker; washing solutions were reserved for fluorescent imaging. At each time point, 1 mL of PECF was added to samples and fully removed to be measured for cumulative release. For the duration of test, the samples were kept at 37°C. Fluorescence of crosslinking, washing, and release solutions were measured via plate reader (Infinite 200 Pro, Tecan, Switzerland), using the experimentally determined calibration curve of fluorescence intensity and FITC-Dextran concentration in PECF medium (Figure 5.2).

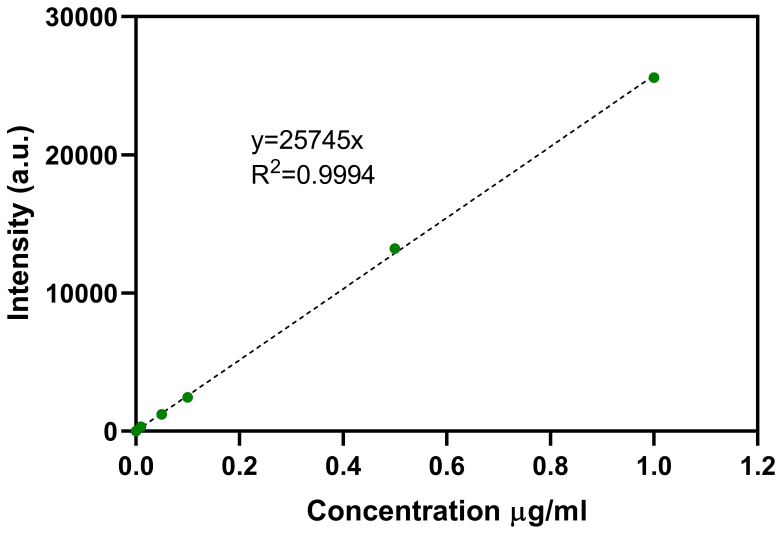

Figure 5.2: Calibration curve of FITC-Dextran in PECF medium (n = 3).

The mass of entrapped FITC-Dextran (M_E) in samples was calculated using Eq. 5.3, where M_{in} is the initially incorporated mass of FITC-Dextran per sample in μg, M_C is the FITC-Dextran measured from crosslinking solutions, M_W is the FITC-Dextran measured from washing solutions, and R is the amount of FITC-Dextran measured during each time point of the release experiment.

$$M_{\mathrm{E}} = M_{\mathrm{in}} - (M_{\mathrm{C}} + M_{\mathrm{W}} + R) \tag{5.3}$$

Over a 2-week period, samples crosslinked for 1 minute showed the highest cumulative release ($84.36 \pm 5.5\%$) of FITC-Dextran into PECF release medium (Figure 5.3). Release from the 1-minute crosslinked samples was significantly higher than 3- and 5-minute crosslinked samples ($48.55 \pm 4.21\%$ and $41.66 \pm 6.73\%$, respectively). No significant difference in cumulative release was observed between 3- and 5-minute crosslinked samples. The high percentage of cumulative release from 1-minute samples points towards the use of these silk coated threads as long-term drug delivery mechanisms, in which an initial burst release may be favored. For example, *in vivo* experimental results by Xie et al. show accelerated wound healing through the promotion of angiogenesis, re-epithelialization, and controlled granulation tissue formation, via the short-term burst release of growth factor, followed by a long-term sustained release [129].

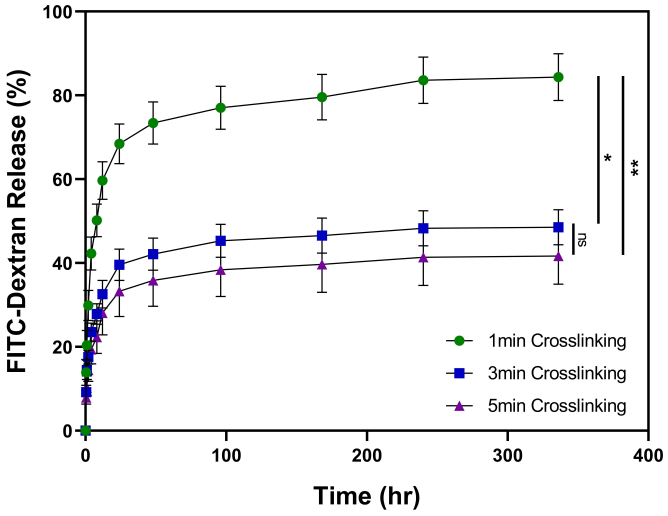

Figure 5.3: 2-week release of FITC-Dextran from silk fibroin with three crosslinking times of 1, 3, and 5 min (n = 3, $p* = 0.0265$, $p** = 00075$).

5.2 Temperature responsive drug release

PNIPAm demonstrates thermoresponsive behavior at 32°C in aqueous solutions, undergoing reversible phase transition in response to environmental temperature change [82]. Release of the two drug models FITC-Dextran and Rhodamine B from PCL/PNIPAm coated threads (spooling velocity = 0 mm/s, ES time = 20 sec, thread-needle distance = 8 cm) was studied at 25 and 37°C. Fluorescence of the release solutions was measured via plate reader using the experimentally determined calibration curve of fluorescence intensity for FITC-Dextran (Figure 5.2) and Rhodamine (Figure 5.4) in PECF medium.

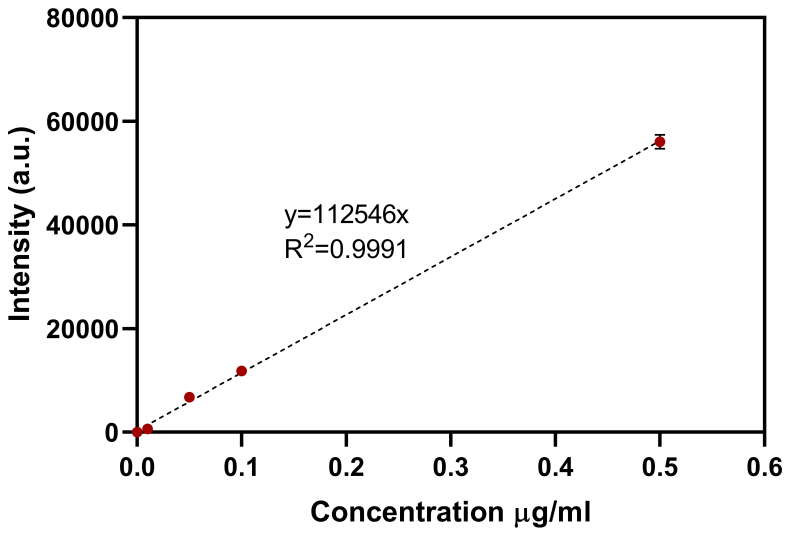

Figure 5.4: Calibration curve of Rhodamine in PECF medium (n = 3).

Figure 5.5 shows the cumulative release of (A) large drug model FITC-Dextran and (B) small drug model Rhodamine from PCL/PNIPAm coated threads at the two temperatures for a period of 120 minutes. After 2 hours, the cumulative release of FITC-Dextran reached 64.55 ± 4.08 and $32.23 \pm 4.28\%$ for 25 and 36°C, respectively. The cumulative release of Rhodamine was lower, and reached 0.475 ± 0.032 and $0.677 \pm 0.082\%$ for 25 and 36°C, respectively. The release of both drug-models

was significantly different for 25 and 37°C ($p* < 0.05$). While both release profiles show an initial burst, this is followed by a period of gradual release. The burst release of FITC-Dextran was observed to occur fully within the first 5 minutes of testing. Hydrophilic small molecule drugs, modelled here with Rhodamine, have high aqueous solubility and are incompatibility with insoluble polymers, which makes their long-term release challenging [130]. Therefore, the lower cumulative release of Rhodamine may be due to the solute-polymer interactions and incompatible solubility parameters of Rh (27.4 MPa) and PCL/PNIPAm (18.25 MPa and 21.9 MPa, respectively) [131]. It has also been shown that fast burst release of drugs from polymeric nanocarriers is a major limitation in achieving controlled drug delivery *in vivo* [132]. To prevent the initial burst releases seen in Figure 5.5A and B, drugs and/or growth factors may instead be loaded in the core of multi-axial nanofibers obtained by coaxial or triaxial electrospinning [84].

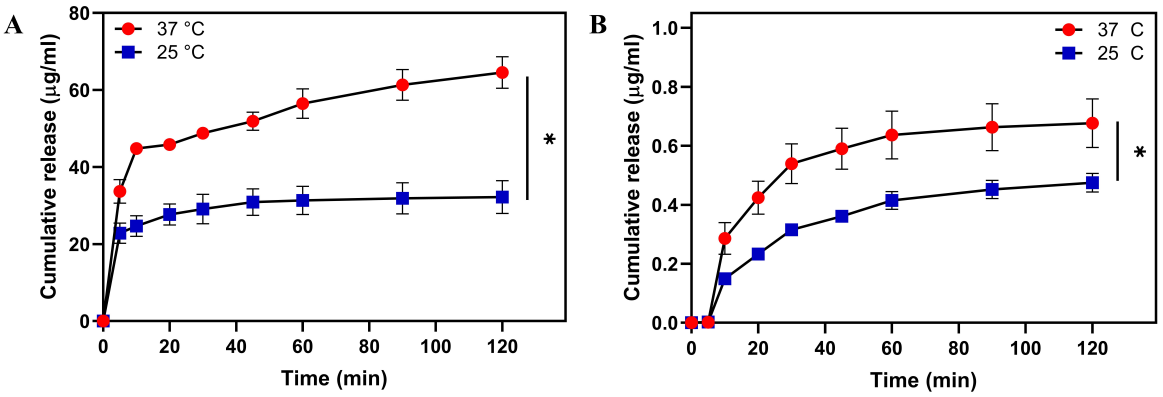

Figure 5.5: (A) FITC-Dextran and (B) Rhodamine release from PCL-PNIPAm coated threads ($p* < 0.05$, n = 3).

5.3 Bacterial study

Drug-loaded electrospun PCL has been widely studied for passive drug releasing applications. For example, Ruckh et al. developed a rifampicin-loaded PCL scaffold for peri-prosthetic infections [133], while others have shown application of electrospun PCL for the support of human cell growth in tissue regeneration [134] and implantable drug delivery systems [135]. The antibacterial activities of PCL/PNIPAm electrospun coated threads were evaluated against model microbial species Gram-negative *Escherichia Coli* (*E. coli*). The application area of such antibiotic-loaded threads is in clinical wound care, where bacterial infections have been shown to significantly decrease wound healing rates [13].

E. coli strains are frequently isolated from skin and soft tissue infections, including surgical and traumatic wounds, foot ulcers, and decubitus ulcers [136]. The administration of the appropriate antibiotic depends upon susceptibility pattern and is important for the treatment of high-risk *E. coli* infections [137]. The chosen antibiotic, doxycycline, was based on previous studies by researchers Lai et al. [137]. Doxycycline is an inexpensive antimicrobial agent that exhibits a broad spectrum of activity against different pathogens, including Gram-negative bacteria such as *E. coli*, and is commonly the drug of choice in the treatment of infectious diseases [138, 137]. This antibiotic drug has also proven to be effective against common multidrug-resistant pathogens such as *A. baumannii*, *P. aeruginosa*, and *S. maltophilia* [137].

5.3.1 Bacterial work

The antibacterial activity of the coated threads was studied using a disk diffusion method. A 100 μL aliquot of bacterial solution (*E. coli*, ATCC, USA), containing 10^8 CFU/mL (colony forming units) previously sub-cultured and reconstituted in

nutrient broth, was spread onto an agar (LB Broth (Lennox) powder medium, Sigma Aldrich) coated petri dish. Antibiotic-loaded samples 1 cm in length were placed on the surfaces of the petri dishes and incubated at 37°C for 24 hr. Electrospun coated thread samples with no loaded antibiotic component were chosen as negative control. Top-down images were taken of the petri dishes and the area of the inhibition zones was measured using image processing software (NIH ImageJ, Version 1.52).

5.3.2 Antibiotic delivery on agar plates

A zone of inhibition (ZOI) test was performed on plain and doxycycline-loaded PCL/PNIPAm coated threads. A statistically significant difference in measured ZOI on cultured plates of *E. coli* occurred between the three concentrations of loaded antibiotic (0, 0.25, and 2.5 μg) (Figure 5.6). No measurable ZOI occurred with plain PCL-PNIPAm coated threads, indicating that the polymers in the coating material did not have any antibacterial effect. The ZOI measured 0.595$\pm$0.099 and 1.196$\pm$0.159 mm^2, for 0.25 μg and 2.5 μg loading, respectively.

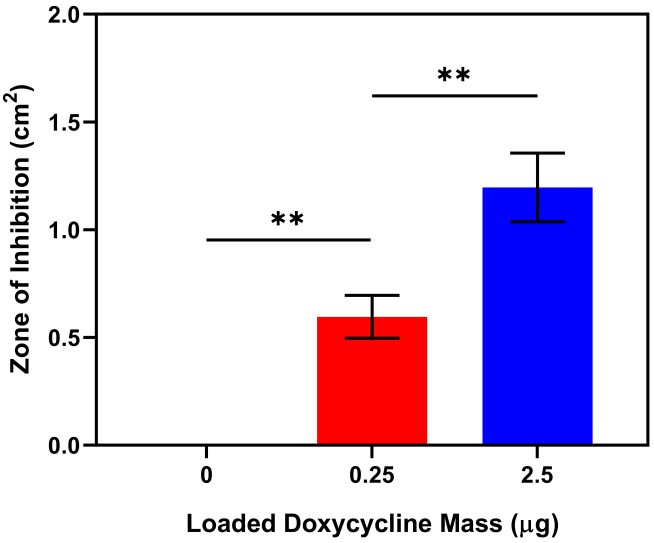

Figure 5.6: Measured ZOI of doxycycline-loaded thread samples (0 μg, (2) 0.25 μg, and (3) 2.5 μg doxycycline) on bacterial culture (n = 3, p$**$ < 0.01, control = electrospun coated thread with no drug component).

5.3.3 Bacterial growth on antibiotic-loaded threads

In this study, plain electrospun PCL/PNIPAm coated threads and electrospun PCL/PNIPAm coated threads loaded with 1 mg/mL doxycycline via direct addition to the ES polymer solution, were fixed for SEM imaging to qualitatively analyze the adherent *E. coli* bacteria after 24 hours. Figure 5.7 shows the result of antibacterial-loaded electrospun coated threads after 24 hr incubation. The rod-shaped bacteria can be seen attached to the electrospun fibers, highlighted in red. With the addition of the antibiotic to the ES solution, significantly fewer bacteria were observed attached to the nanofiber scaffold after the incubation period (Figure 5.7B). In comparison, non-loaded coated threads visibly showed more adherent bacteria on the electrospun scaffold (Figure 5.7A).

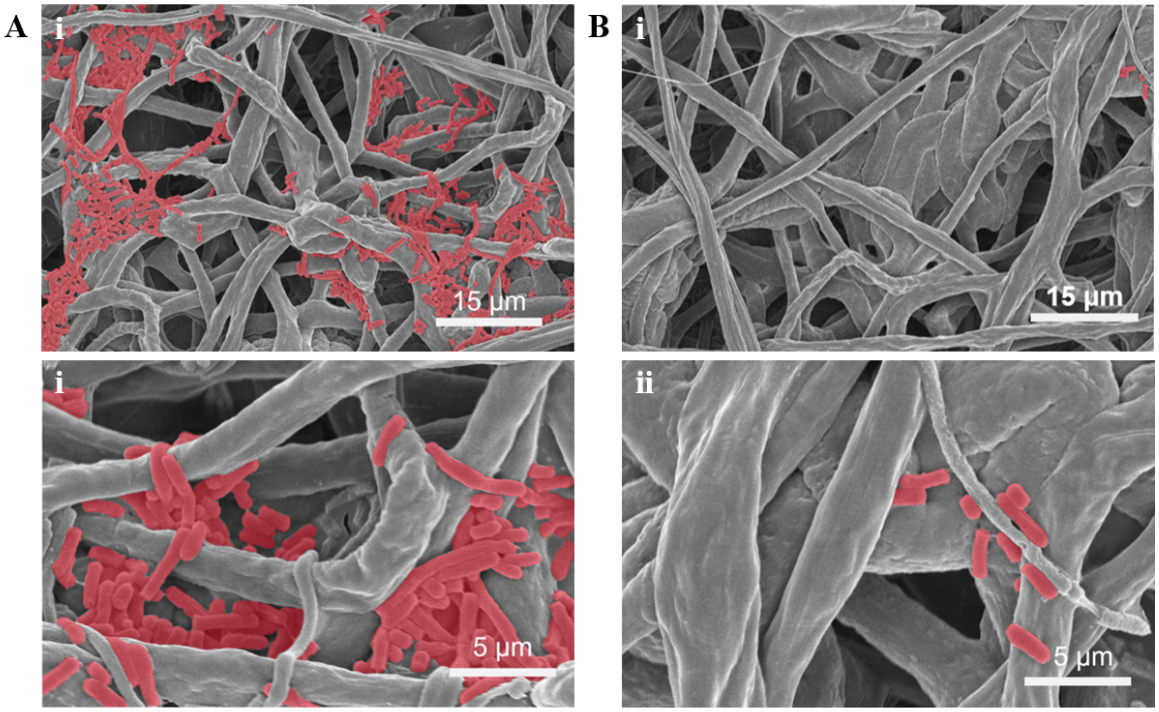

Figure 5.7: Bacterial culture on (A) (i) plain PCL/PNIPAm coated threads, (ii) magnified, and (B) (i) Antibiotic-loaded PCL/PNIPAm coated threads, (ii) magnified (bacteria highlighted in red).

Chapter 6

In vitro cell study

The *in vitro* cell viability and proliferation of HaCaT cells on electrospun coated threads was studied to demonstrate the use of these threads for tissue engineering applications. As stated in Chapter 3, a variety of textile methods can be utilized to combine coated threads into complex structures and geometries; high and low cell proliferation would play an important role in the spatially patterned growth of cells for specific applications, while high viability is essential for the success of the engineered tissue construct and for implantable suture devices. Physical cues are important factors in tissue development and in controlling cell function, which has been demonstrated through the use of geometrically patterned substrates [139]. Ingber, Whitesides et al. demonstrated the use of patterned substrates for controlling the microenvironment of individual cells [140]. The degree of cell spreading, which led to a higher degree of cytoskeleton tension and differential expression, was controlled by micro-island size patterning [141].

Biocompatibility concerns exist with these threads in suture, engineered tissues, and biosensor applications when directly or indirectly in contact with the organism and/or cells. Gelatin is a natural component of the extracellular matrix, and fab-

ricated electrospun scaffolds have been shown to provide a suitable ground for cell adhesion, proliferation, and differentiation [142]. Silk fibroin was also expected to have high viability, as researchers have previously shown that the biological functionality of the natural polymer silk fibroin enhances HaCaT viability, which is attributable to the material-cell interactions [65, 143]. Additionally, randomly oriented electrospun silk fibroin fibers have been shown to improve cell viability in artificial extracellular matrices for tissue engineering applications [144]. While still a biocompatible material, PCL has been regularly combined with other materials such as graphene [145], gelatin [146], PLLA and PLGA (poly(lactic-co-glycolic acid)) [147], to enhance the hydrophilicity and cell attachment of various cell lines on fabricated scaffolds for hard and soft tissue engineering applications.

6.1 *In vitro* biocompatibility

High cell viability requirements exist for these nanofibrous coated threads for applications where they are in direct or indirect contact with cells and tissues. A cell viability experiment was performed with HaCaT cells (a spontaneously transformed aneuploid immortal keratinocyte cell line) to determine the biocompatibility of three electrospun polymer (gelatin, silk fibroin, and PCL) coated thread types. This cell line was chosen as keratinocytes play an important role in wound healing and re-epithelialization [148].

6.1.1 Cell viability experiment

Human primary keratinocytes (HaCaT; Addexbio, USA, Catalog No. T0020001) were cultured in Dulbecco's modified eagle's medium (DMEM; Gibco™, ThermoFisher Scientific, USA) supplemented with 10% fetal bovine serum (Gibco™, ThermoFisher

Scientific, USA) and 1% penicillin-streptomycin (Gibco^{TM}, ThermoFisher Scientific, USA). The cells were cultured in cell culture flasks (T75, VWR,USA) until they reached 80-90% confluence and were detached using Trypsin-EDTA (0.5%, Gibco^{TM}, ThermoFisher Scientific, USA) prior to seeding on the electrospun coated threads. Coated thread samples were placed in nonadherent PDMS-coated wells, to which 50 μL cell suspension containing 1,000,000 cells was added, with the subsequent addition of 950 μL cell media after 2 hours.

The viability of cells grown on the coated threads after 3 and 7 days was determined by a flow cytometer (Attune NxT, ThermoFisher Scientific, USA). To this end, cells were initially detached from the threads as described above and stained with Live/Dead viability kit (Invitrogen, ThermoFisher Scientific, USA) according to the protocol provided by the supplier. Briefly, 2 and 4 μL of 50 μM calcein and 2 mM ethidium homodimer-1 solutions, respectively, were added to the cell suspension detached from the electrospun coated threads. After 15-20 minutes of incubation at room temperature in a dark condition, analysis of stained cells was carried out by the flow cytometer using 488 nm excitation and measuring green fluorescence emission for calcein (530/30 nm bandpass) and red fluorescence emission for ethidium homodimer-1 (610/20 nm bandpass). Finally, the live and dead populations were gated to exclude debris from the plots, as seen in Figure 7.1.

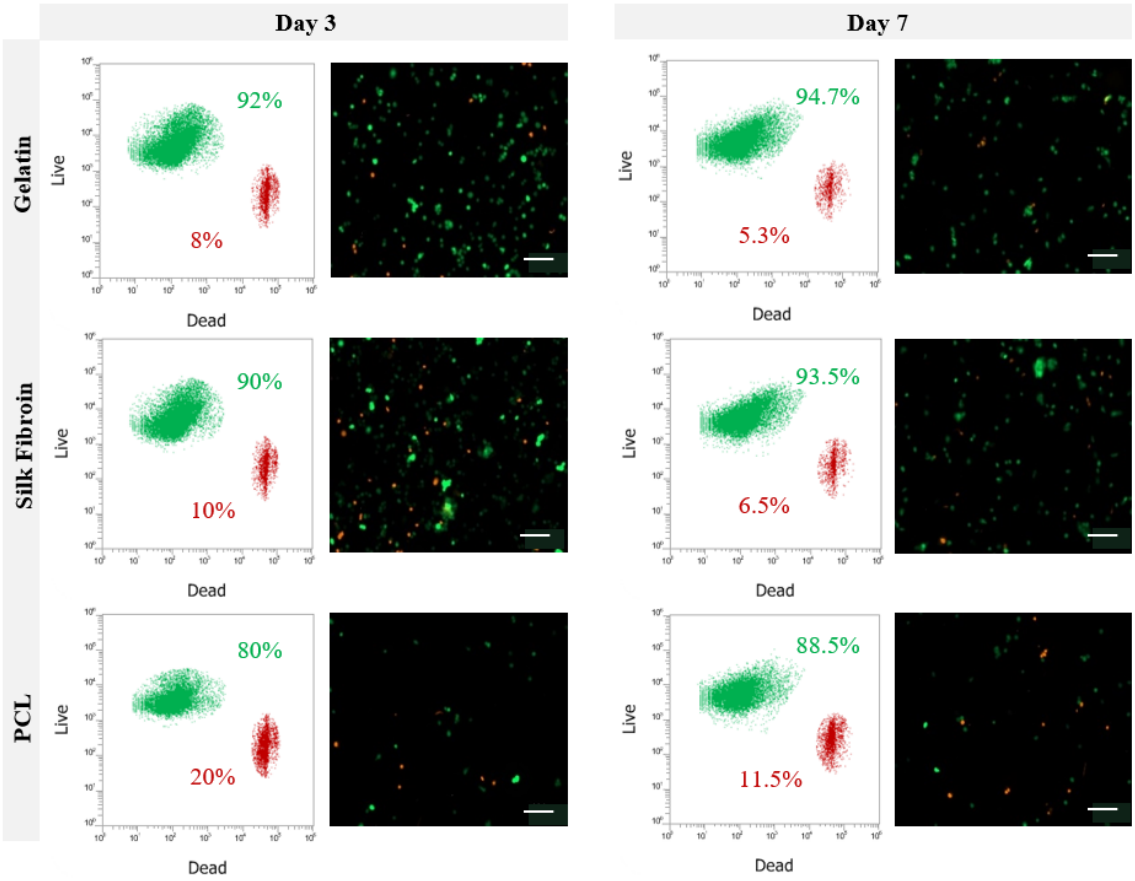

Figure 6.1: Gated dot plot of Live/Dead fluorescence showing number of live and dead HaCaT cell populations at days 3 and 7, and the corresponding Live/Dead assay for the cells detached from gelatin, silk fibroin, and PCL samples (scale bars = 100 μm).

6.1.2 *In vitro* biocompatibility results

The viability in percentage of live HaCaT cells was measured at days 3 and 7. Cell viability was determined as per Eq. 7.1, where N_L is the number of live cells and N_D is the number of dead cells.

$$Viability\% = \frac{N_L}{N_L + N_D} \times 100 \tag{6.1}$$

In Figure 7.2, the observed percentage of dead cells relative to the number of living cells decreased for the three sample groups between days 3 and 7. The numerical

Live/Dead results show that the number of live cells significantly increased between days 3 and 7, for the gelatin, silk fibroin, and PCL sample types ($p****< 0.0001$, $p*** = 0.0007$, $p* = 0.0117$, respectively). Additionally, gelatin and silk fibroin coated samples demonstrated higher viability ($94.7 \pm 0.35\%$, $93.47 \pm 0.30\%$, respectively) than PCL ($88.5 \pm 1.99\%$) at day 7. The high viability and biocompatibility of the gelatin and silk fibroin polymer coated threads point towards their use as scaffolding materials of 3D tissue engineering scaffolds assembled using textile-based methods. Additionally, the relatively high viability for all three sample types show that the proposed electrospinning fabrication and crosslinking processes do not negatively impact biocompatibility or the ES coated sutures or result in cytotoxic residues.

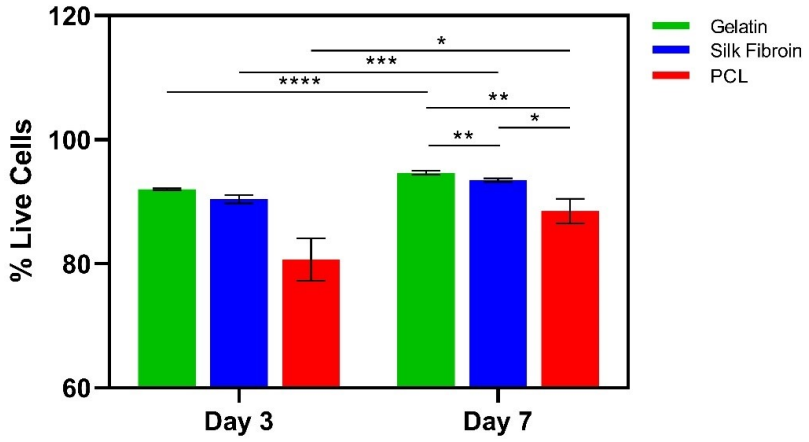

Figure 6.2: Percentage of live cells of plain, plain carbon coated, PCL coated, gelatin coated, and silk fibroin coated threads at days 3 and 7 (n = 3, p**** <0.0001, $p*** = 0.0007$, $p* = 0.0117$).

6.2 *In vitro* cell attachment & proliferation

HaCaT cells were similarly used to quantitatively study cell attachment and proliferation on coated threads, for the applications of tissue engineered constructs and suture materials. The three common electrospun polymer types PCL, gelatin, and

silk fibroin were studied. Cell adherence to a scaffold substrate is a fundamental preliminary step for further cell-substrate interactions for promoting cell proliferation, migration, and differentiation [149]. High rates of cell proliferation on silk fibroin scaffolds have been demonstrated by multiple research groups [65, 150, 151]. While the gelatin samples crosslinked with glutaraldehyde vapor become more water-resistant, the nanofibrous structure of electrospun gelatin has been found to enhance cell adhesion and proliferation [152]. Additionally, gelatin possesses the RGD (arginine-glycine-aspartic acid) sequences of collagen, which makes it highly effective for cell adhesion [152]. Other than the hydrophobic and nonspecific binding of cells to electrospun PCL samples, PCL is intrinsically hydrophobic [153] and lacks functional groups such as RGD-motif-containing cell-attachment peptides that provide specific binding sites for cells [154, 155]. Additionally, the differences in electrospun fiber diameter and resulting surface topography between silk fibroin, gelatin, and PCL samples may have affected the cell morphology and cell proliferation [156].

6.2.1 Cell attachment experiment

Three samples with (1 cm in length) were placed in each well of a 24-well plate coated with non-adherent agarose. Cell seeding was carried out by adding 50 mL of a cell suspension that contained 1,000,000 HaCaT cells in culture media. After two hours of incubation, 950 μL of culture media was added to have the final volume of 1 mL. 24 hours after seeding the cells, the threads were gently washed with culture media twice to remove non-adhered cells and the cells were treated with 250 μL of Trypsin-EDTA (0.25%) for 15 minutes to detach cells from the surface of threads. 500 μL of cell media was then added to deactivate the Trypsin-EDTA followed by centrifugation of the supernatant at 300 g to make a cell pellet. The supernatant was then removed, and the cell pellet was resuspended in 1 mL of cell culture media. Finally, 10 μL of cell

suspension was stained with Trypan Blue (Gibco^{TM}, ThermoFisher Scientific, USA) and the number of cells was counted using a hemocytometer.

6.2.2 Cell proliferation experiment

The proliferation rate of HaCaT cells on gelatin, silk fibroin, and PCL coated samples after 1, 3, and 7 days was calculated by measuring the metabolic activity of cells at these time points. Cells were seeded on three 1 cm-long threads per well, as described previously. At the specific time points, the culture media was replaced by the PrestoBlue solution and incubated for 30 minutes. 100 μL of supernatant was removed from each well and plated in a 96-well plate. Fluorescence intensity was measured at excitation (560 nm) and emission wavelengths (590 nm) using a microplate reader. The relative proliferation rate was calculated by normalizing the measured intensity at each condition with respect to the condition with the lowest intensity.

6.2.3 Cell attachment & proliferation results

The cell proliferation for the three electrospun polymers (gelatin, silk fibroin, and PCL) measured at days 1, 3, and 7 in relative fluorescent units, is seen in Figure 7.3A. Over the 7 day duration, proliferation for all three polymer coated thread samples increased significantly. As expected, PCL coated threads demonstrated significantly lower proliferation compared to gelatin and silk fibroin samples ($p****< 0.0001$, $p*** < 0.001$, respectively). At day 1, gelatin and silk fibroin coated samples also demonstrated significantly different total cell proliferation, with silk fibroin having the highest proliferation of the three sample types ($p* < 0.05$).

The relative cell attachment on the surface of gelatin and silk fibroin coated threads after 24 hours was not significantly different. Given the hydrophobic nature

and the lack of cell-binding motifs on PCL electrospun nanofibers, the cell attachment on the PCL coated samples was found to be significantly lower than gelatin and silk fibroin, as shown in Figure 7.3B ($p** < 0.01$). This low cell attachment of PCL coated threads may however be beneficial for applications where low cell adhesion is preferable. For example, specific wound dressings and non-absorbable removable sutures may require low cell adhesion to improve the removal procedure and reduce patient pain.

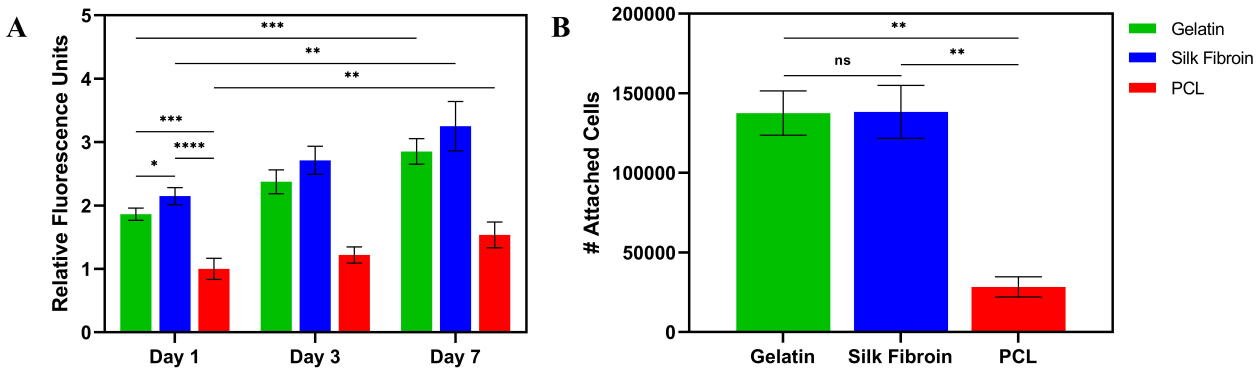

Figure 6.3: (A) Cell proliferation on gelatin, silk fibroin, and PCL electrospun coated threads, at days 1, 3, and 7. (B) Cell attachment on gelatin, silk fibroin, and PCL electrospun coated threads at 24hr ($p* < 0.05$, $p** < 0.01$, $p*** < 0.001$, $p**** < 0.0001$).

6.3 Attached cell morphology

A cell morphology experiment was performed with fibroblast cells, which play a central role in wound healing and are among the most common cells of connective tissues in humans. The experiment was performed to examine the attached cell morphology on three electrospun polymer coated sample types, gelatin, silk fibroin, and PCL. Samples consisted of simple electrospun mats instead of coated threads to reduce the chance of SEM image distortion from the curved thread surfaces. Fibrob-

lasts were chosen for cell culture due to the ease of culture and their presence in tissue injury [157, 158].

6.3.1 Cell culture

Human normal dermal fibroblasts (Normal, Human, Adult; ATCC, USA) cells were cultured in DMEM, supplemented with 10% fetal bovine, and 1% penicillin-streptomycin. 100,000 dermal fibroblast cells were seeded onto square electrospun mats of silk, gelatin, and PCL. After 24 hours, the mats were washed three times with warmed, fresh DMEM to remove non-adhered cells from the surface of the samples. Afterwards, cells were fixed with 3.7 vv% formaldehyde (VWR, Radnor, USA) for 15 minutes at room temperature, followed by triple rinsing of the cells with PBS (phosphate-buffered saline).

6.3.2 Attached cell imaging results

The morphology of cells was visualized in SEM images. These images in Figure 7.4 show fibroblast cell attachment on (A) gelatin, (B) silk fibroin, and (C) PCL coated threads. Noticeably fewer cells were seen attached to the PCL sample, compared to silk fibroin and gelatin samples. The fibroblast cells growing on gelatin and silk-fibroin nanofibers exhibit more isotropic morphologies on the randomly oriented fibers, with clear borders between the cells and the nanofibers, in comparison to the PCL sample images. Fibroblasts on PCL samples had elongated morphologies which may be due to the hydrophobic nature of PCL.

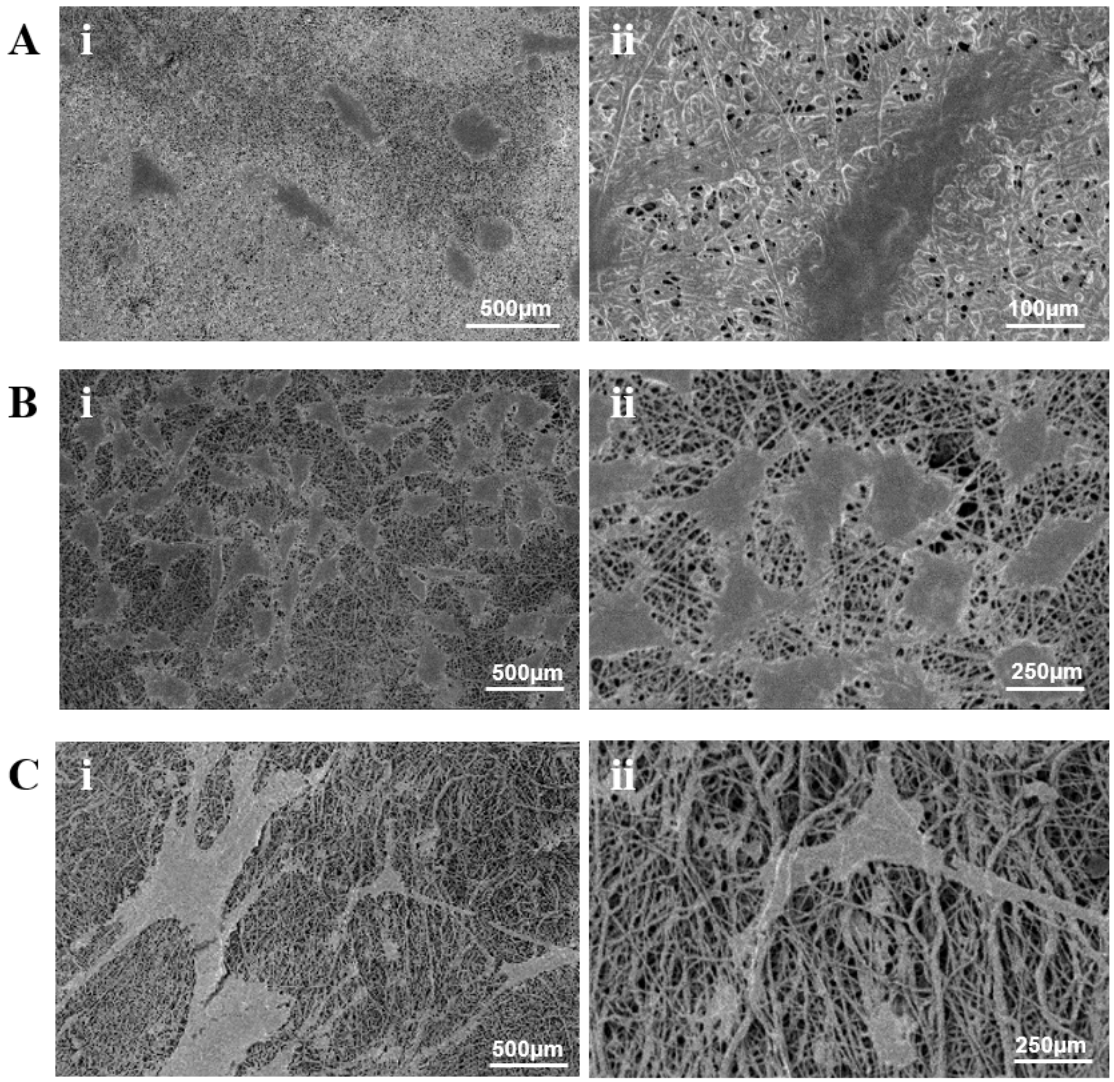

Figure 6.4: SEM images of cell attachment on (A) (i) gelatin, (ii) magnified to show cell morphology, (B) (i) silk fibroin coated threads, (ii) magnified, and (C) (i) PCL coated thread, (ii) magnified.

Chapter 7

Conclusions

Advancements in the miniaturization of biosensors and drug release systems have altered the health care system by allowing for the continuous monitoring of patients' health status. Fabrication methods such as photolithography, screen-printing, and stamping, are common approaches for the implementation of biosensors onto planar and flexible surfaces, while localized drug dosing requirements have driven micro- and nano-fabricated implantable drug delivery systems such as microfluidics, microneedles, and micropumps, fabricated using traditional lithography processes. These traditional microfabrication methods often are costly and time consuming, however. Threads are an alternative base material for biosensor and drug releasing systems with considerable economical and scalability benefits. Further, while threads have been traditionally used in the apparel and textile industries, they have recently emerged as promising scaffolding material candidates for engineered tissue constructs and biomedical implants for organ replacement and repair.

Clinical sutures are mainly used for the physical approximation of tissues, but recent growth in the development of new suture materials for improved healing outcomes through surface modification plays upon the inherent versatility of the thread tech-

nology. When a foreign object such as a suture material is introduced to a wound for wound closure, the body's inflammatory reaction will initiate a chain of inflammation. Findings suggest that different commercial suture materials induce both differentiated tissue reactions and morphological surface changes, and that tissue reactions must be individualized. Such patient-individualization of suture properties can be achievable through the use of suture coatings.

The inherent versatility of ES technology in terms of polymer molecular properties, fiber size, structure, morphology, alignment, porosity, makes this technique highly effective for the preparation of various nanostructures for biomedical applications. ES has been widely used within the area of biomedical and tissue engineering given its compatibility with a range of synthetic and natural biocompatible polymers. Additionally, the high adaptability of ES technologies and the commercial economical of thread-based biotechnologies make their combination of significant research interest. In this thesis, a novel ES fabrication method was developed for creating electrospun coated threads and sutures and was evaluated as a proof-of-concept study. The developed ES method allowed for the continuous fabrication of multifunctional sutures and threads with a wide range of polymers and important biological characteristics. The proposed ES system incorporated spooling threads with an ES spinerette, which caused electrospun nanofibers to collect onto the surface of the thread. The coating layer thickness and the alignment of the nanofibers with the direction of the thread was tunable with respect to run time, spooling velocity, and the displacement between the spinerette needle and the thread. Multi-layer coated threads were also demonstrated, allowing for the combination of polymers with different properties and characteristics. The flexibility of the nanofibrous coated threads offers easy manipulation with different materials (e.g. skin, textile-based wound dressings) and allowed the threads to be combined into three dimensional constructs.

Electrospun coated stimuli-responsive thread-based structures were coated with ES polymers that respond to induced or natural changes in the surrounding environment. Electrically conductive and magnetized threads were fabricated with the addition of conductive polymer PEDOT and Iron (III) Oxide MNPs to ES solutions, and the response of these threads to electric, temperature, RH, and magnetic field stimuli was characterized. The ES coating method was then applied to passive drug release and on demand drug release and evaluated for efficiency. Passive drug release was shown to occur due to degradation of nanofibrous coatings, dependant on the degree of the electrospun fiber crosslinking. Further, a composite ES polymer containing a thermoresponsive material was studied for temperature-dependant drug release. Both the cumulative release and release rate of two drug models from these electrospun coatings proved significantly different, demonstrating future use of these materials temperature-stimulated drug release. To determine the efficacy of these nanofibrous sutures against Gram-negative *E. coli* bacterial infections, electrospun coatings were actively loaded with the antibiotic doxycycline. The functionalized samples displayed positive antibacterial properties when tested against E. coli in a ZOI test and with qualitative SEM imaging. HaCaT cell viability and fibroblast cell proliferation and attachment on three coated suture types (silk fibroin, gelatin, and PCL) was studied. The different electrospun polymer coatings offered high cell viability and varying levels of cell attachment for application-dependant flexibility. These results outlined in this thesis indicate that the developed ES thread coating fabrication method is largely applicable to a wide range of biomedical engineering application areas, driven by the flexibility and scalability of the combined ES and thread-based technologies. The fabricated smart multifunctional sutures and threads were proven to perform in the niches of biosensor miniaturization, targeted drug delivery systems, and tissue engineering.

Future directions of this work of this work include applying the electrospun coated threads to expanded areas of application of biological testing and drug-delivery. On-demand temperature-controlled drug release is an important next step utilizing the thermoresponsive PCL/PNIPAm/PEGDA ES polymer coating. With the incorporation of 5% PEGDA in the ES solution, and subsequent crosslinking using UV light, the point of drug release from threads can be increased above 37°C (body temperature). A thermally conductive electrode prepared through dip coating in conductive inks can be coated with the given drug-loaded PCL/PNIPAm/PEGDA polymer and be used to induce a localized temperature change at the site of delivery. Such conductive ink-dipped heating threads, used with temperature-responsive drug releasing materials for on-demand drug release for wound healing applications, have been shown to cause an unwanted inflammatory response in a previous *in vivo* study, due to the thermally conductive ink component. By coating the heating threads in ES materials, that wound healing outcomes are hypothesized to improve in terms of wound closure and inflammatory response. As a future direction of this work, the proposed thread-based heating system can be tested *in vivo* on animal models to determine biocompatibility and inflammatory response. Moreover, the proposed fabrication system can be used for the further development of biosensing ES coated threads. For example, diabetes mellitus can cause inflammation and chronic non-healing of wounds. The surveillance of such high-risk wounds using glucose sensors may help improve wound healing outcomes. Glucose sensing threads may utilize the addition of glucose oxidase (GOx) to the ES polymer, catalyzing the oxidation of β-D-glucose by producing hydrogen peroxide (H_2O_2), which can be measured at a reference electrode. Using chronoamperometry, the current at the electrode would be measurable and proportional to the number of glucose molecules present in the blood supply to the wound, therefore allowing for faster diagnosis and treatment.

Bibliography

[1] C. C. Chu, *Biotextiles as Medical Implants*. Woodhead Publishing, 2013.

[2] D. H. Reneker and A. L. Yarin, "Electrospinning jets and polymer nanofibers," *Polymer*, vol. 49, no. 10, pp. 2387–2425, 2008.

[3] A. Theron, E. Zussman, and A. L. Yarin, "Electrostatic field-assisted alignment of electrospun nanofibres," *Nanotechnology*, vol. 12, no. 3, pp. 384–390, 2001.

[4] W. E. Teo and S. Ramakrishna, "Electrospun fibre bundle made of aligned nanofibres over two fixed points," *Nanotechnology*, vol. 16, no. 9, p. 1878, 2005.

[5] C. Zhang, C. Gao, M.-W. Chang, Z. Ahmad, and J.-S. Li, "Continuous micron-scaled ropes comprising two intercalated fibers are fabricated via a modified multinozzle rotating spinneret," *Appl Phys Lett*, vol. 109, 2016.

[6] C. Dennis, S. Sethu, S. Nayak, L. Mohan, Y. Morsi, and G. Manivasagam, "Suture materials — current and emerging trends," *J Biomed Mater Res A*, vol. 104, no. 6, 2016.

[7] F. Selvi, S. Cakarer, T. Can, S. I. Kirli Topcu, A. Palancioglu, B. Keskin, B. Bilgic, M. Yaltirik, and C. Keskin, "Effects of different suture materials on tissue healing," *J Istanb Univ Fac Dent*, vol. 50, no. 1, pp. 35–42, 2016.

[8] D. Geiger, E. S. Debus, U. E. Ziegler, A. Larena-Avellaneda, M. Frosch, A. Thiede, and U. A. Dietz, "Capillary activity of surgical sutures and suture-dependent bacterial transport: a qualitative study," *Surg Infect*, vol. 6, no. 4, pp. 377–83, 2005.

[9] A. Schneider and H. Feussner, *Biomedical Engineering in Gastrointestinal Surgery*. Elsevier Inc., 2017.

[10] J. Zaruby, K. Gingras, J. Taylor, and D. Maul, "An in vivo comparison of barbed suture devices and conventional monofilament sutures for cosmetic skin closure: biomechanical wound strength and histology," *Aesthet Surg J*, vol. 31, no. 2, pp. 232–40, 2011.

[11] G. C. Gurtner, S. Wener, Y. Barrandon, and M. T. Longaker, "Wound repair and regeneration," *Nature*, vol. 453, pp. 314–321, 2008.

[12] H. Sorg, D. J. Tilkorn, S. Hager, J. Hauser, and U. Mirastschijski, "Skin wound healing: An update on the current knowledge and concepts," *Eur Surg Res*, vol. 58, no. 1-2, pp. 81–94, 2017.

[13] R. G. Frykberg and J. Banks, "Challenges in the treatment of chronic wounds," *Adv Wound Care*, vol. 4, no. 9, pp. 560–582, 2015.

[14] A. M. Lock, R. Gao, D. Naot, B. Coleman, J. Cornish, and D. S. Musson, "Induction of immune gene expression and inflammatory mediator release by commonly used surgical suture materials: an experimental in vitro study," *Patient Saf Surg*, vol. 11, no. 1, 2017.

[15] S. Guo and L. A. Dipietro, "Factors affecting wound healing," *J Dent Res*, vol. 89, no. 3, pp. 219–29, 2010.

[16] C. R. Uff, A. D. Scott, A. G. Pockley, and R. K. Phillips, "Influence of soluble suture factors on in vitro macrophage function," *Biomaterials*, vol. 16, no. 5, pp. 355–60, 1995.

[17] M. G. Andrade, R. Weissman, and S. R. Reis, "Tissue reaction and surface morphology of absorbable sutures after in vivo exposure," *J Mater Sci Mater Med*, vol. 17, no. 10, pp. 949–61, 2006.

[18] R. Salcido, "Healing by intention," *Adv Skin Wound Care*, vol. 30, no. 6, pp. 246–247, 2017.

[19] K. E. Johnson and T. A. Wilgus, "Vascular endothelial growth factor and angiogenesis in the regulation of cutaneous wound repair," *Adv Wound Care*, vol. 3, no. 10, pp. 647–661, 2014.

[20] D.-H. Kin, S. Wang, H. Keum, R. Gahaffari, Y.-S. Kim, H. Tao, B. Panilaitis, M. Li, Z. Kang, F. Omenetto, Y. Huang, and J. A. Rogers, "Thin, flexible sensors and actuators as 'instrumented' surgical sutures for targeted wound monitoring and therapy," *Small*, vol. 8, no. 21, pp. 3263–3268, 2012.

[21] E. Meng and T. Hoang, "Micro- and nano-fabricated implantable drug-delivery systems," *Ther Deliv*, vol. 3, no. 12, pp. 1457–67, 2012.

[22] P. Mostafalu, M. Akbari, K. A. Alberti, Q. Xu, A. Khademhosseini, and S. R. Sonkusale, "A toolkit of thread-based microfluidics, sensors, and electronics for 3d tissue embedding for medical diagnostics," *Microsyst Nanoeng*, vol. 2, p. 16039, 2016.

[23] Y. Wang, S. Shang, and C. Li, "Aligned biomimetic scaffolds as a new tendency in tissue engineering," *Curr Stem Cell Res Ther*, vol. 11, no. 1, p. 3, 2016.

[24] L. Magnan, G. Labruni, M. Fenelon, N. Dusserre, M.-P. Foulc, and M. Lafourcade, "Human textiles: A cell-synthesized yarn as a truly "bio" material for tissue engineering applications," *Acta Biomater*, vol. 105, pp. 111–120, 2020.

[25] J. L. Makridakis, G. D. Pins, T. Dominko, and R. L. Page, "Design of a novel engineered muscle construct using muscle derived fibroblastic cells seeded onto braided collagen threads," 2009.

[26] Y. Wu, L. Wang, B. Guo, and P. X. Ma, "Interwoven aligned conductive nanofiber yarn/hydrogel composite scaffolds for engineered 3d cardiac anisotropy," *ACS Nano*, vol. 11, no. 6, pp. 5646–5659, 2017.

[27] S. Barrientos, H. Brem, O. Stojadinovic, and M. Tomic-Canic, "Clinical application of growth factors and cytokines in wound healing," *Wound Repair Regen*, vol. 22, no. 5, pp. 569–78, 2014.

[28] H. Brem and M. Tomic-Canic, "Cellular and molecular basis of wound healing in diabetes," *J Clin Invest*, vol. 117, no. 5, pp. 1219–22, 2007.

[29] N. R. Johnson and Y. Wang, "Drug delivery systems for wound healing," *Curr Pharm Biotechnol*, vol. 16, no. 7, pp. 621–9, 2015.

[30] M. L. Hakim, N. Nahar, M. Saha, M. S. Islam, H. M. Reza, and S. M. Sharker, "Local drug delivery from surgical thread for area-specific anesthesia," *Biomed Phys Eng Express*, vol. 6, no. 1, 2020.

[31] C. L. He, Z. M. Huang, and X. J. Han, "Fabrication of drug-loaded electrospun aligned fibrous threads for suture applications," *J Biomed Mater Res A*, vol. 89, no. 1, pp. 80–95, 2009.

[32] E. J. Torres-Martinez, J. M. C. Bravo, A. S. Medina, G. L. P. Gonzalez, and L. J. V. Gomex, "A summary of electrospun nanofibers as drug delivery system:

Drugs loaded and biopolymers used as matrices," *Curr Drug Deliv*, vol. 15, pp. 1360–1374, 2018.

[33] M. C. Da Silva, R. D. C. A. Leal, H. N. Da Silva, and M. V. L. Fook, "Biodegradable suture threads as controlled drug delivery systems," *Mater Res Innov*, vol. 24, no. 3, pp. 161–165, 2020.

[34] Y. H. Wu, D. G. Yu, H. C. Li, and D. N. Feng, "Electrospun nanofibers for fast dissolution of naproxen prepared using a coaxial process with ethanol as a shell fluid," *Appl Mech Mater*, vol. 662, pp. 29–32, 2014.

[35] G. Piccirillo, D. A. Carvajal Berrio, A. Laurita, A. Pepe, B. Bochicchio, K. Schenke-Layland, and S. Hinderer, "Controlled and tuneable drug release from electrospun fibers and a non-invasive approach for cytotoxicity testing," *Sci Rep*, vol. 9, no. 1, p. 3446, 2019.

[36] T. Potrč, S. Baumgartner, R. Roškar, O. Planinšek, Z. Lavrič, and K. J, "Electrospun polycaprolactone nanofibers as a potential oromucosal delivery system for poorly water-soluble drugs," *Eur J Pharm Sci*, vol. 75, pp. 101–113, 2015.

[37] X. Weng, Y. Kang, Q. Guo, B. Peng, and H. Jiang, "Recent advances in thread-based microfluidics for diagnostic applications," *Biosens Bioelectron*, vol. 132, pp. 171–185, 2019.

[38] M. Mehrali, S. Bagherifard, M. Akbari, A. Thakur, B. Mirani, M. Mehrali, M. Hasany, G. Orive, P. Das, J. Emneus, T. L. Andresen, and A. Dolatshahi-Pirouz, "Blending electronics with the human body: A pathway toward a cybernetic future," *Adv Sci*, vol. 5, no. 10, p. 1700931, 2018.

[39] M. Sekar, M. Pandiaraj, S. Bhansali, N. Ponpandian, and C. Viswanathan, "Carbon fiber based electrochemical sensor for sweat cortisol measurement," *Sci Rep*, vol. 9, no. 1, p. 403, 2019.

[40] S. S. Banerjee, A. Roychowdhury, N. Taneja, R. Janrao, J. Khandare, and D. Paul, "Chemical synthesis and sensing in inexpensive thread-based microdevices," *Sens Actuators B Chem*, vol. 186, pp. 439–445, 2013.

[41] A. Tamayol, M. Akbari, N. Annabi, A. Paul, A. Khademhosseini, and D. Juncker, "Fiber-based tissue engineering: Progress, challenges, and opportunities," *Biotechnol Adv*, vol. 31, no. 5, pp. 669–87, 2013.

[42] B. B. Mollet, I. L. J. Bogaerts, G. C. van Almen, and P. Y. W. Dankers, "A bioartificial environment for kidney epithelial cells based on a supramolecular polymer basement membrane mimic and an organotypical culture system," *J Tissue Eng Regen Med*, vol. 11, no. 6, pp. 1820–1834, 2017.

[43] H. Ramakrishna, T. Li, T. He, J. Temple, M. W. King, and A. Spagnoli, "Tissue engineering a tendon-bone junction with biodegradable braided scaffolds," *Biomater Res*, vol. 23, p. 11, 2019.

[44] G. Chen, T. Sato, H. Ohgushi, T. Ushida, T. Tateishi, and J. Tanaka, "Culturing of skin fibroblasts in a thin plga–collagen hybrid mesh.," *Biomaterials*, vol. 26, no. 15, pp. 2559–2566, 205.

[45] J. L. Chen, Z. Yin, W. L. Shen, X. Chen, B. C. Heng, X. H. Zou, and H. W. Ouyang, "Efficacy of hesc-mscs in knitted silk-collagen scaffold for tendon tissue engineering and their roles," *Biomaterials*, vol. 31, no. 9438-9451, 2010.

[46] Y. Li, F. Guo, Y. Hao, S. K. Gupta, J. Hu, Y. Wang, N. Wang, Y. Zhao, and M. Guo, "Helical nanofiber yarn enabling highly stretchable engineered microtissue," *Proc Natl Acad Sci USA*, vol. 116, no. 19, pp. 9245–9250, 2019.

[47] M. Ebrahimi, S. Ostrovidov, S. Salehi, S. B. Kim, H. Bae, and A. Khademhosseini, "Enhanced skeletal muscle formation on microfluidic spun gelatin methacryloyl (gelma) fibres using sur," *J Tissue Eng Regen Med*, vol. 12, no. 11, pp. 2151–2163, 2018.

[48] A. Y. Hsiao, T. Okitsu, H. Onoe, M. Kiyosawa, H. Teramae, S. Iwanaga, T. Kazama, T. Matsumoto, and S. Takeuchi, "Smooth muscle-like tissue constructs with circumferentially oriented cells formed by the cell fiber technology," *PLoS One*, vol. 10, no. 3, p. e0119010, 2015.

[49] N. S. Taheri, Y. Wang, and K. J. Berean, "Lithium intercalated molybdenum disulfide-coated cotton thread as a viable nerve tissue scaffold candidate," *ACS Appl Nano Mater*, vol. 2, no. 4, pp. 2044–2053, 2019.

[50] Q. Fang, D. Chen, Z. Yang, and M. Li, "In vitro and in vivo research on using antheraea pernyi silk fibroin as tissue engineering tendon scaffolds," *Mater Sci Eng*, vol. 29, no. 5, pp. 1527–1534, 2009.

[51] T. J. Sill and H. A. von Recum, "Electrospinning: applications in drug delivery and tissue engineering," *Biomaterials*, vol. 29, no. 13, pp. 1989–2006, 2008.

[52] M. Wang and Q. Zhao, *Encyclopedia of Biomedical Engineering*, vol. 1. Elsevier, 2019.

[53] J. H. Wendorff, S. Agarwal, and A. Grenier, *Electrospinning: Materials, Processing, and Applications*. Wiley-VCH, 2012.

[54] N. Tucker, J. J. Stranger, M. P. Staiger, H. Razzaq, and K. FHofman, "The history of the science and technology of electrospinning from 1600 to 1995," *J Eng Fiber Fabr*, vol. 7, no. 2, pp. 63–73, 2012.

[55] A. Haider, S. Haider, and I.-K. Kang, "A comprehensive review summarizing the effect of electrospinning parameters and potential applications of nanofibers in biomedical and biotechnology," *Arab J Chem*, vol. 11, no. 8, pp. 1165–1188, 2018.

[56] L. Liverani and A. R. Boccaccini, "Electrospinning with benign solvents: feasibility study and versatile use of poly(epsilon-caprolactone) fibers," 2016.

[57] B. Sundaray, V. Subramanian, T. S. Natarajan, R.-Z. Xiang, C.-C. Shang, and W.-S. Fann, "Electrospinning of continuous aligned polymer fibers," *Appl Phys Lett*, vol. 84, 2004.

[58] B. Zhang, X. Yan, Y. Xy, H.-S. Zhao, M. Yu, and Y.-L. Long, "Measurement of adhesion of in situ electrospun nanofibers on different substrates by a direct pulling method," *Adv Mater Sci Eng*, 2020.

[59] D. Li, Y. Wang, and Y. Xia, "Electrospinning nanofibers as uniaxially aligned arrays and layer-by-layer stacked films," *Adv Mater*, vol. 16, no. 4, pp. 261–366, 2004.

[60] J. Xue, T. Wu, Y. Dai, and Y. Xia, "Electrospinning and electrospun nanofibers: Methods, materials, and applications," *Chem Rev*, vol. 119, no. 8, pp. 5298–5415, 2019.

[61] J.-M. Bourget, M. Guillemette, T. Veres, F. A. Auger, and L. Germain, *Alignment of Cells and Extracellular Matrix Within Tissue-Engineered Substitutes*. IntechOpen, 2013.

[62] Z. Wei, W. Zhao, Y. Wang, X. Wang, S. Long, and J. Yang, "Novel pnipam-based electrospun nanofibres used directly as a drug carrier for "on-off" switchable drug release," *Colloids Surf B*, vol. 182, 2019.

[63] C. Pignatelli, G. Perotto, M. Nardini, R. Cancedda, M. Mastrogiacomo, and A. Athanassiou, "Electrospun silk fibroin fibers for storage and controlled release of human platelet lysate," *Acta Biomater*, vol. 73, pp. 365–376, 2018.

[64] H. R. Munj, J. J. Lannutti, and D. L. Tomasko, "Understanding drug release from pcl/gelatin electrospun blends," *J Biomater Appl*, vol. 31, no. 6, pp. 933–949, 2016.

[65] G. Carrasco-Torres, M. A. Valdes-Madrigal, V. R. Vasquez-Garzon, R. Baltierrez-Hoyos, E. De la Cruz-Burelo, R. Roman-Doval, and A. A. Valencia-Lazcano, "Effect of silk fibroin on cell viability in electrospun scaffolds of polyethylene oxide," *Polymers*, vol. 11, no. 3, 2019.

[66] G. Yang, K. L. Kampstra, and M. R. Abidian, "High-performance conducting polymer nanofiber biosensors for detection of biomolecules," *Adv Mater*, vol. 26, no. 29, pp. 4954–4960, 2014.

[67] P. Heikkila, A. Sipila, M. Peltola, A. Harlin, and A. Taipale, "Electrospun pa-66 coating on textile surfaces," *Text Res J*, vol. 77, no. 11, pp. 864–870, 2007.

[68] E. Zussman, A. Theron, and A. L. Yarin, "Formation of nanofiber crossbars in electrospinning," *Appl Phys Lett*, vol. 82, no. 6, p. 973, 2003.

[69] J. Zheng, X. Yan, M.-m. Li, G.-F. Yu, H.-D. Zhang, W. Pisula, X.-X. He, J.-L. Duvail, and Y.-Z. Long, "Electrospun aligned fibrous arrays and twisted ropes: Fabrication, mechanical and electrical properties, and application in strain sensors," *Nanoscale Res Lett*, vol. 10, p. 475, 2015.

[70] L. Huang, K. Nagapudi, and Apk, "Engineered collagen–peo nanofibers and fabrics," *J Biomater Sci Polym Ed*, vol. 12, no. 9, pp. 979–993, 2001.

[71] S. Y. Chew, Y. Wen, Y. Dzenis, and K. W. Leong, "The role of electrospinning in the emerging field of nanomedicine," *Curr Pharm Des*, vol. 12, no. 36, pp. 4751–70, 2006.

[72] B. M. Whited and M. N. Rylander, "The influence of electrospun scaffold topography on endothelial cell morphology, alignment, and adhesion in response to fluid flow," *Biotechnol Bioeng*, vol. 111, no. 1, pp. 184–95, 2014.

[73] S. Megelski, J. S. Stephens, D. B. Chase, and J. F. Rabolt, "Micro- and nanostructured surface morphology on electrospun polymer fibers," *Macromolecules*, vol. 35, no. 22, pp. 8456–8466, 2002.

[74] M. J. Mochane, T. S. Motsoeneng, E. R. Sadiku, T. C. Mokhena, and J. S. Sefadi, "Morphology and properties of electrospun pcl and its composites for medical applications: A mini review," *Appl Sci*, vol. 9, no. 11, 2019.

[75] E. Malikmammadov, T. E. Tanir, A. Kiziltay, V. Hasirci, and N. Hasirci, "Pcl and pcl-based materials in biomedical applications," *J Biomater Sci Polym Ed*, vol. 29, no. 7-9, pp. 863–893, 2018.

[76] J. M. Hackett, T. T. Dang, E. V. Tsai, and X. Cao, "Electrospun biocomposite polycaprolactone/collagen tubes as scaffolds for neural stem cell differentiation," *Materials*, vol. 3, no. 6, pp. 3714–3728, 2010.

[77] D. J. Hines and D. L. Kaplan, "Mechanisms of controlled release from silk fibroin films," *Biomacromolecules*, vol. 12, no. 3, pp. 804–12, 2011.

[78] G. H. Altman, F. Diaz, C. Jakuba, T. Calabro, R. L. Horan, J. Chen, H. Lu, J. Richmond, and D. L. Kaplan, "Silk-based biomaterials," *Biomaterials*, vol. 24, no. 3, pp. 401–416, 2003.

[79] S. Mohammadzadehmoghadam and Y. Dong, "Fabrication and characterization of electrospun silk fibroin/gelatin scaffolds crosslinked with glutaraldehyde vapor," *Front Mater*, vol. 6, no. 91, 2019.

[80] P. Sajkiewicz and D. Kolbuk, "Electrospinning of gelatin for tissue engineering – molecular conformation as one of the overlooked problems," *J Biomater Sci Polym Ed*, vol. 25, no. 18, pp. 2009–2022, 2014.

[81] M. A. Oraby, A. I. Waley, A. I. El-Dewany, E. A. Saad, and B. M. Abd El-Hady, "Electrospinning of gelatin functionalized with silver nanoparticles for nanofiber fabrication," *Model Numer Simul Mater Sci*, vol. 3, no. 4, pp. 5094–5102, 2013.

[82] H. G. Shchild, "Poly(n-isopropylacrylamide): experiment, theory and application," *Prog Polym Sci*, vol. 17, no. 2, pp. 163–249, 1992.

[83] A. C. B. Allen, E. Barone, C. Crosby, L. J. Suggs, and J. Zoldan, "Electrospun poly(n-isopropyl acrylamide)/ poly(caprolactone) fibers for the generation of anisotropic cell sheets†," *Biomaterials*, vol. 5, no. 8, pp. 1661–1669, 2017.

[84] T. Tran, M. Hernandez, D. Patel, E. Burns, V. Peterman, and J. Wu, "Controllable and switchable drug delivery of ibuprofen from temperature responsive composite nanofibers," *Nano Converg*, vol. 2, no. 15, 2015.

[85] H. Kotturi, A. Abuabed, H. Zafar, E. Sawyer, B. Pallipparambil, H. Jamadagni, and M. Khandaker, "Evaluation of polyethylene glycol diacrylate-polycaprolactone scaffolds for tissue engineering applications," *J Funct Biomater*, vol. 8, no. 3, 2017.

[86] Y. Ji, K. Ghosh, B. Li, J. C. Sokolov, R. A. Clark, and M. H. Rafailovich, "Dual-syringe reactive electrospinning of cross-linked hyaluronic acid hydrogel nanofibers for tissue engineering applications," *Macromol Biosci*, vol. 6, no. 10, pp. 811–7, 2006.

[87] H. R. Ashjari, A. Ahmadi, and M. S. S. Dorraji, "Synthesis and employment of pegda for fabrication of superhydrophilic pvdf/pegda electrospun nanofibrous membranes by in-situ visible photopolymerization," *Korean J Chem Eng*, vol. 35, no. 1, pp. 289–297, 2018.

[88] C.-K. Cho, W.-J. Hwang, K. Eun, S.-H. Choa, S.-I. Na, and H.-K. Kim, "Mechanical flexibility of transparent pedot:pss electrodes prepared by gravure printing for flexible organic solar cells," *Sol Energy Mater Sol Cells*, vol. 95, no. 12, pp. 3269–3275, 2011.

[89] B. Bessaire, M. Mathieu, V. Salles, T. Yeghoyan, C. Celle, J. P. Simonato, and A. Brioude, "Synthesis of continuous conductive pedot:pss nanofibers by electrospinning: A conformal coating for optoelectronics," *ACS Appl Mater Inter*, vol. 9, no. 1, pp. 950–957, 2017.

[90] H. E. Schneider, J. G. Steuber, W. Du, M. Mortazavi, and D. W. Bullock, "Polyethylene oxide nanofiber production by electrospinning," *J AR Acad Sci*, vol. 70, 2016.

[91] S. Ramakrishna, K. Fujihara, W.-E. Teo, T.-C. Lim, and Z. Ma, *An Introduction to Electrospinning and Nanofibers*. World Scientific Publishing Co., 2005.

[92] J. Pelipenki, J. Kristl, B. Jankovic, S. Baumgartner, and P. Kocbek, "The impact of relative humidity during electrospinning on the morphology and me-

chanical properties of nanofibers," *Int J Pharm*, vol. 456, no. 1, pp. 125–143, 2013.

[93] W. He and R. Benson, *Applied Plastics Engineering Handbook*. Plastics Design Library, Elsevier, 2 ed., 2017.

[94] Z. Hadisi, J. Nourmohammadi, and J. Mohammadi, "Composite of porous starch-silk fibroin nanofiber-calcium phosphate for bone regeneration," *Ceram Int*, vol. 41, no. 9, pp. 10745–10754, 2015.

[95] R. Jayakumar and S. Nair, eds., *Biomedical Applications of Polymeric Nanofibers*, vol. 246 of *Adv Polym Sci*. Springer, 2012.

[96] G.-T. Kim, Y.-J. Hwang, Y.-C. Ahn, H.-S. Shin, J.-K. Lee, and C.-M. Sung, "The morphology of electrospun polystyrene fibers," *Korean J Chem Eng*, vol. 22, no. 1, pp. 147–153, 2005.

[97] H. S. Salehhudin, E. N. Mohamad, W. N. L. Mahadi, and A. M. Afifi, "Multiple-jet electrospinning methods for nanofiber processing: A review," *Mater Manuf Process*, vol. 33, no. 5, pp. 479–498, 2017.

[98] N. M. Neves, R. Campos, A. Pedro, J. Cunha, F. Macedo, and R. L. Reis, "Patterning of polymer nanofiber meshes by electrospinning for biomedical applications," *Int J Nanomedicine*, vol. 2, no. 3, pp. 433–48, 2007.

[99] M. Afshari, ed., *Electrospun Nanofibers*. Textiles, Woodhead Publishing, 2017.

[100] J. A. Matthews, G. E. Wnek, D. G. Simpson, and G. L. Bowlin, "Electrospinning of collagen nanofibers," *Biomacromolecules*, vol. 3, no. 2, pp. 232–8, 2002.

[101] E. D. Boland, G. E. Wnek, D. G. Simpson, K. J. Pawlowski, and G. L. Bowlin, "Tailoring tissue engineering scaffold using electrostatic processing techniques:

A study of poly(glycolic acid) electrospinning," *J Macromol Sci A*, vol. 38, no. 12, 2001.

[102] C. Pailler-Mattei, S. Bec, and H. Zahouani, "In vivo measurements of the elastic mechanical properties of human skin by indentation tests," *Med Eng Phys*, vol. 30, no. 5, pp. 599–606, 2008.

[103] P. G. Agache, C. Monneur, J. L. Leveque, and J. De Rigal, "Mechanical properties and young's modulus of human skin in vivo," *Arch Dermatol Res*, vol. 269, no. 3, pp. 221–32, 1980.

[104] J. Hochberg, K. M. Meyer, and M. D. Marion, "Suture choice and other methods of skin closure," *Surg Clin North Am*, vol. 89, no. 3, pp. 627–41, 2009.

[105] M. Akbari, A. Tamayol, S. Bagherifard, L. Serex, P. Mostafalu, N. Faramarzi, M. H. Mohammadi, and A. Khademhosseini, "Textile technologies and tissue engineering: A path toward organ weaving," *Adv Healthc Mater*, vol. 5, no. 7, pp. 751–66, 2016.

[106] H. Chen, A. Malheiro, C. van Blitterswijk, C. Mota, P. A. Wieringa, and L. Moroni, "Direct writing electrospinning of scaffolds with multidimensional fiber architecture for hierarchical tissue engineering," *ACS Appl Mater Inter*, vol. 9, no. 44, pp. 38187–38200, 2017.

[107] M. Akbari, A. Tamayol, S. Bagherifard, L. Serex, P. Mostafalu, N. Faramarzi, M. H. Mohammadi, and A. Khademhosseini, "Textile technologies and tissue engineering: A path towards organ weaving," *Adv Healthc Mater*, vol. 5, no. 7, pp. 751–766, 2017.

[108] D. H. Xu, Z. Zhu, and Y. Fang, "The effect of a common antibiotics doxycycline on non-healing chronic wound," *Curr Pharm Biotechnol*, vol. 18, no. 5, pp. 360–364, 2017.

[109] N. Huebsch, P. R. Arany, A. S. Mao, D. Shvartsman, O. A. Ali, S. A. Bencherif, J. Rivera-Feliciano, and D. J. Mooney, "Harnessing traction-mediated manipulation of the cell/matrix interface to control stem-cell fate," *Nat Mater*, vol. 9, no. 6, pp. 518–26, 2010.

[110] A. Summerfield, F. Meurens, and M. E. Ricklin, "The immunology of the porcine skin and its value as a model for human skin," *Mol Immunol*, vol. 66, no. 1, pp. 14–21, 2015.

[111] V. Dini, P. Salvo, A. Janowska, F. Di Francesco, A. Barbini, and M. Romanelli, "Correlation between wound temperature obtained with an infrared camera and clinical wound bed score in venous leg ulcers," *Wounds*, vol. 27, no. 10, pp. 274–278, 2015.

[112] A. Chanmugam, D. Langemo, K. Thomason, E. Altenburger, A. Tippett, L. Henderson, and T. Zortman, "Relative temperature maximum in wound infection and inflammation as compared with a control subject using long-wave infrared thermography," *Adv Skin Wound Care*, vol. 30, no. 9, pp. 406–414, 2017.

[113] K. Cutting, "Wound exudate: Composition and functions," *Brit J Comm Nurs*, vol. 8, no. 1, 2003.

[114] Y. F. Wang, T. Sekine, Y. Takeda, K. Yokosawa, H. Matsui, D. Kumaki, T. Shiba, T. Nishikawa, and S. Tokito, "Fully printed pedot:pss-based temper-

ature sensor with high humidity stability for wireless healthcare monitoring," *Sci Rep*, vol. 10, no. 1, p. 2467, 2020.

[115] I. W. Kwon, H. J. Son, W. Y. Kim, Y. S. Lee, and H. C. Lee, "Thermistor behavior of pedot:pss thin film," *Synth Mater*, vol. 159, no. 12, pp. 1174–1177, 2009.

[116] L. V. Kayser and D. J. Lipomi, "Stretchable conductive polymers and composites based on pedot and pedot:pss," *Adv Mater*, vol. 31, no. 10, p. e1806133, 2019.

[117] L. Biebmann, L. P. Kreuzer, T. Widmann, N. Hohn, J.-F. Moulin, and P. Muller-Buschbaum, "Monitoring the swelling behavior of pedot:pss electrodes under high humidity conditions," *ACS Appl Mater Inter*, vol. 10, no. 11, pp. 9865–9872, 2018.

[118] J. L. Corchero and A. Villaverde, "Biomedical applications of distally controlled magnetic nanoparticles," *Trends Biotechnol*, vol. 27, no. 8, pp. 468–76, 2009.

[119] T. K. Jain, M. K. Reddy, M. A. Morales, D. L. Leslie-Pelecky, and V. Labhasetwar, "Biodistribution, clearance, and biocompatibility of iron oxide magnetic nanoparticles in rats," *Mol Pharm*, vol. 5, no. 2, pp. 316–27, 2008.

[120] X. Zhao, J. Kim, C. A. Cezar, N. Huebsch, K. Lee, K. Bouhadir, and D. J. Mooney, "Active scaffolds for on-demand drug and cell delivery," *Proc Natl Acad Sci U S A*, vol. 108, no. 1, pp. 67–72, 2011.

[121] Y. Wei, X. Zhang, Y. Song, B. Han, X. Hu, X. Wang, Y. Lin, and X. Deng, "Magnetic biodegradable fe3o4/cs/pva nanofibrous membranes for bone regeneration," *Biomed Mater*, vol. 6, no. 5, p. 055008, 2011.

[122] J. Meng, Y. Zhang, X. Qi, H. Kong, C. Wang, Z. Xu, S. Xie, N. Gu, and H. Xu, "Paramagnetic nanofibrous composite films enhance the osteogenic responses of pre-osteoblast cells," *Nanoscale*, vol. 2, no. 12, pp. 2565–9, 2010.

[123] M. Banobre-Lopez, Y. Pineiro-Redondo, M. Sandri, A. Tampieri, R. De Santis, V. A. Dediu, and J. Rivas, "Hyperthermia induced in magnetic scaffolds for bone tissue engineering," *IEEE T Magn*, vol. 50, no. 11, 2014.

[124] A. Tampieri, T. D'Alessandro, M. Sandri, S. Sprio, E. Landi, L. Bertinetti, S. Panseri, G. Pepponi, J. Goettlicher, M. Banobre-Lopez, and J. Rivas, "Intrinsic magnetism and hyperthermia in bioactive fe-doped hydroxyapatite," *Acta Biomater*, vol. 8, no. 2, pp. 843–51, 2012.

[125] I. Negut, V. Grumezescu, and A. M. Grumezescu, "Treatment strategies for infected wounds," *Molecules*, vol. 23, no. 9, 2018.

[126] F. Zhang, J. N. Wang, and B. Q. Zuo, "Effect of aqueous ethanol treatment on the electrospun sf nanofiber mats," 2010.

[127] S. Fathollahipour, A. A. Mehrizi, A. Ghaee, and M. Koosha, "Electrospinning of pva/chitosan nanocomposite nanofibers containing gelatin nanoparticles as a dual drug delivery syst," *J Biomed Mater Res*, pp. 3852–3862, 2015.

[128] Z. Hadisi, J. Nourmohammadi, and S. M. Nassiri, "The antibacterial and anti-inflammatory investigation of lawsonia inermis-gelatin-starch nano-fibrous dressing in burn wound," *Int J Biol Macromol*, vol. 107, no. Pt B, pp. 2008–2019, 2018.

[129] Z. Xie, C. B. Paras, H. Weng, P. Punnakitikashem, L. C. Su, K. Vu, L. Tang, J. Yang, and K. T. Nguyen, "Dual growth factor releasing multi-functional nanofibers for wound healing," *Acta Biomater*, vol. 9, no. 12, pp. 9351–9, 2013.

[130] S. F. Chou, D. Carson, and K. A. Woodrow, "Current strategies for sustaining drug release from electrospun nanofibers," *J Control Release*, vol. 220, no. Pt B, pp. 584–91, 2015.

[131] H. Munj, J. Lannutti, and D. Tomasko, "Understanding drug release from pcl/gelatin electrospun blends," *J Biomat App*, vol. 31, no. 6, pp. 933–949, 2016.

[132] K. E. Uhrich, S. M. Cannizzaro, R. S. Langer, and K. M. Shakesheff, "Polymeric systems for controlled drug release," *Chem Rev*, vol. 99, no. 11, pp. 3181–98, 1999.

[133] T. T. Ruckh, R. A. Oldinski, D. A. Carroll, K. Mikhova, J. D. Bryers, and K. C. Popat, "Antimicrobial effects of nanofiber poly(caprolactone) tissue scaffolds releasing rifampicin," *J Mater Sci Mater Med*, vol. 23, no. 6, pp. 1411–20, 2012.

[134] E. Zdraveva, B. Mijovic, E. G. Bajsic, I. Silvac, T. H. Grguric, and A. Tomlijenovic, "Electrospun pcl/cefuroxime scaffolds with custom tailored topography," *J Exp Nanosci*, vol. 14, no. 1, pp. 41–55, 2019.

[135] Y. Gao, T. W. Teoh, Q. Wnag, and G. R. Williams, "Electrospun organic–inorganic nanohybrids as sustained release drug delivery systems," *J Mater Chem*, no. 46, pp. 9165–9174, 2017.

[136] Z. Petkovsek, K. Elersic, M. Gubina, D. Zgur-Bertok, and M. Starcic Erjavec, "Virulence potential of escherichia coli isolates from skin and soft tissue infections," *J Clin Microbiol*, vol. 47, no. 6, pp. 1811–7, 2009.

[137] C.-C. Lai, C.-C. Chen, H.-L. Huang, Y.-C. Chuang, and H.-T. Tang, "The role of doxycycline in the therapy of multidrug-resistant e. coli – an in vitro study," *Sci Rep*, vol. 6, 2016.

[138] G. Zhanel, K. Homenuik, K. Nichol, A. Noreddin, L. Vercaigne, J. Embil, A. Gin, J. A. Karlowsky, and D. J. Hoban, "The glycylcyclines: a comparative review with the tetracyclines," *Drugs*, vol. 64, no. 1, 2004.

[139] K. A. Kilian, B. Bugarija, B. T. Lahn, and M. Mrksich, "Geometric cues for directing the differentiation of mesenchymal stem cells," *Proc Natl Acad Sci USA*, vol. 107, no. 11, pp. 4872–7, 2010.

[140] C. S. Chen, M. Mrksich, S. Huang, G. M. Whitesides, and D. E. Ingber, "Geometric control of cell life and death," *Science*, vol. 276, no. 5317, pp. 1425–8, 1997.

[141] K. Bhadriraju, M. Yang, S. A. Ruiz, D. Pirone, J. Tan, and C. S. Chen, "Activation of rock by rhoa is regulated by cell adhesion, shape, and cytoskeletal tension," *Exp Cell Res*, vol. 313, no. 16, pp. 3636–3623, 2008.

[142] Y. Zhang, H. Ouyang, C. T. Lim, S. Ramakrishna, and Z. M. Huang, "Electrospinning of gelatin fibers and gelatin/pcl composite fibrous scaffolds," *J Biomed Mater Res B Appl Biomater*, vol. 72, no. 1, pp. 156–65, 2005.

[143] S. Yan, Q. Zhang, J. Wang, Y. Liu, S. Lu, M. Li, and D. L. Kaplan, "Silk fibroin/chondroitin sulfate/hyaluronic acid ternary scaffolds for dermal tissue reconstruction," *Acta Biomater*, vol. 9, no. 6, pp. 6771–82, 2013.

[144] N. Kasoju and U. Bora, "Silk fibroin based biomimetic artificial extracellular matrix for hepatic tissue engineering applications," *Biomed Mater*, vol. 7, no. 4, 2012.

[145] W. Wang, G. Caetano, W. S. Ambler, J. J. Blaker, M. A. Frade, P. Mandal, C. Diver, and P. Bartolo, "Enhancing the hydrophilicity and cell attachment of

3d printed pcl/graphene scaffolds for bone tissue engineering," *Materials*, vol. 9, no. 12, 2016.

[146] D. Rong, P. Chen, Y. Yang, Q. Li, W. Wan, X. Fang, J. Zhang, Z. Han, J. Tian, and J. Ouyang, "Fabrication of gelatin/pcl electrospun fiber mat with bone powder and the study of its biocompatibility," *J Funct Biomater*, vol. 7, no. 1, 2016.

[147] T. Suga, N. T. Xuyen, K. Matsumoto, M. Jikei, K. Takahashi, H. Kubota, and T. Tamura, "Enhanced proliferation of hela cells on plla-pcl and plga-pcl multiblock copolymers," *Polym J*, vol. 49, pp. 567–573, 2017.

[148] J. Kopp, G. Y. Wang, P. Kulmburg, S. D. Ge, S. Dooley, and R. E. Horch, "Accelerated wound healing by in vivo application of keratinocytes overexpressing kgf," *Mol Ther*, vol. 10, no. 1, pp. 86–96, 2004.

[149] A. Taubert, J. F. Mano, and J. C. Rodríguez-Cabello, eds., *Biomaterials Surface Science*. John Wiley & Sons, 2013.

[150] Y. Qi, H. Wang, K. Wei, Y. Yang, R. Y. Zheng, I. S. Kim, and K. Q. Zhang, "A review of structure construction of silk fibroin biomaterials from single structures to multi-level structures," *Int J Mol Sci*, vol. 18, no. 3, 2017.

[151] L. Meinel, S. Hofmann, V. Karageorgiou, C. Kirker-Head, J. McCool, G. Gronowicz, L. Zichner, R. Langer, G. Vunjak-Novakovic, and D. L. Kaplan, "The inflammatory responses to silk films in vitro and in vivo," *Biomaterials*, vol. 26, no. 2, pp. 147–55, 2005.

[152] S.-C. Wu, W.-H. Chang, G.-C. Dong, K.-Y. Chen, Y.-S. Chen, and C.-H. Yao, "Cell adhesion and proliferation enhancement by gelatin nanofiber scaffolds," *J Bioact Compat Polym*, vol. 26, no. 6, pp. 565–577, 2011.

[153] J. S. Ferreira, S. Gomes, C. Henriques, J. P. Borges, and J. C. Silva, "Electrospinning polycaprolactone dissolved in glacial acetic acid: Fiber production, nonwoven characterization, and in vitro evaluation," *Appl Polym*, vol. 131, no. 22, 2014.

[154] M. Gabriel, G. P. van Nieuw Amerongen, V. W. Van Hinsbergh, A. V. Amerongen, and A. Zentner, "Direct grafting of rgd-motif-containing peptide on the surface of polycaprolactone films," *J Biomater Sci Polym Ed*, vol. 17, no. 5, pp. 567–77, 2006.

[155] D. Mondal, M. Griffith, and S. S. Venkatraman, "Polycaprolactone-based biomaterials for tissue engineering and drug delivery: Current scenario and challenges," *Int J Polymeric Mat*, vol. 65, no. 5, pp. 255–265, 2016.

[156] A. S. Badami, M. R. Kreke, M. S. Thompson, J. S. Riffle, and A. S. Goldstein, "Effect of fiber diameter on spreading, proliferation, and differentiation of osteoblastic cells on electrospun poly(lactic acid) substrates," *Biomaterials*, vol. 27, no. 4, pp. 596–606, 2006.

[157] B. Alberts, A. Johnson, and L. J, *Fibroblasts and Their Transformations: The Connective-Tissue Cell Family*. Molecular Biology of the Cell, New York: Garland Science, 4 ed., 2002.

[158] P. Bainbridge, "Wound healing and the role of fibroblasts," *J Wound Care*, vol. 22, no. 8, pp. 407–408, 2013.